

Wave Propagation in a Strongly Nonlinear Locally Resonant Granular Crystal

K. Vorotnikov* and Y. Starosvetsky

Faculty of Mechanical Engineering, Technion Israel Institute of Technology, Technion City, Haifa 32000, Israel

G. Theocharis

*Laboratoire d'Acoustique de l'Université du Maine,
UMR-CNRS 6613, Av. Olivier Messiaen, Le Mans 72000, France*

P.G. Kevrekidis

Department of Mathematics and Statistics, University of Massachusetts, Amherst MA 01003-4515, USA

In this work, we study the wave propagation in a recently proposed acoustic structure, the locally resonant granular crystal. This structure is composed of a one-dimensional granular crystal of hollow spherical particles in contact, containing linear resonators. The relevant model is presented and examined through a combination of analytical approximations (based on ODE and nonlinear map analysis) and of numerical results. The generic dynamics of the system involves a degradation of the well-known traveling pulse of the standard Hertzian chain of elastic beads. Nevertheless, the present system is richer, in that as the primary pulse decays, secondary ones emerge and eventually interfere with it creating modulated wavetrains. Remarkably, upon suitable choices of parameters, this interference “distills” a weakly nonlocal solitary wave (a “nanopteron”). This motivates the consideration of such nonlinear structures through a separate Fourier space technique, whose results suggest the existence of such entities not only with a single-side tail, but also with periodic tails on both ends. These tails are found to oscillate with the intrinsic oscillation frequency of the out-of-phase motion between the outer hollow bead and its internal linear attachment.

I. INTRODUCTION

Dynamics of one-dimensional granular chains has attracted substantial interest from the researchers of quite different scientific areas [1–24] due to their exciting dynamical properties. These chains support the formation of highly robust, strongly localized and genuinely traveling elastic stress waves. The existence of traveling waves was originally proved in [7] using the variational approach of [25], yet no information was given on their profile. Their single pulse character (in the strain variables) was rigorously shown in [26], following the approach of [27], and the doubly exponential character of their spatial decay in the absence of precompression was established. Earlier work on the basis of long wavelength approximations and numerical computations had conjectured that the waves were genuinely compact (spanning a finite number of elements) [1].

Recent studies [9–18] in the area have been mainly concerned with the effect of various types of structural inhomogeneities induced in the granular chain. The latter leads to a modulation of the solitary waves, as well as to new kinds of breathing modes produced either robustly [12–14, 28, 29] or transiently [30]. Wave propagation in tapered and decorated granular chains has been extensively studied in [9–11] both analytically and numerically. The approximations developed in these works for the estimation of the maximal pulse velocity recorded on each one of the granules along with its propagation through such inhomogeneous granular chains have demonstrated a good correspondence of the analytic predictions with the numerical simulations. Additional experimental, computational and analytical studies were devoted to the dynamics of the periodic granular chains (e.g. diatomic chains, granular containers, etc.) under various conditions of initial pre-compression [12–18]. Dynamics of primary pulses in the non-compressed granular chain perturbed by a weak dissipation has been considered in [19–24]. These, in turn, shed light on the evolution of the primary pulses in the dissipative, 1D granular media and provide some qualitative theoretical (in some cases in connection with experiments [23]) estimations for modeling the dissipation in the chain as well as depicting the rate of decay of the primary pulse. A systematic theoretical attempt to capture the (decaying) evolution of a primary pulse in the granular chain subject to on-site perturbation has been provided in the extensive study of [31].

In the present paper we study a novel acoustic structure which has been recently considered in some experimental and theoretical studies [32–34], the locally resonant granular crystal. The fundamental unit cell of these periodic systems is made of an outer mass (hollow spherical shell and an inner mass connected by a linear spring). Our

*Corresponding author; Electronic address: kirill.vorotnikov@inria.fr

principal aim is to examine the dynamics of this novel class of chains, as regards their ability to propagate travelling waves in the presence of these internal resonators. What we generally observe in this setting is a decay of the principal pulse (in the strain variables), due to its coupling to the internal variables. The rate of such decay of a primary pulse can be fully captured analytically. Perhaps even more importantly, we show that, depending on the parameters of the internal resonator (i.e. coupling stiffness and mass), the response can range from the above mentioned (continuous) decay, to the formation of a genuinely travelling primary pulse. The latter scenario is examined in close detail and is identified as a case example of a “nanopterion” solution, whose tail carries an oscillation with the intrinsic linear frequency of the system (of the relative motion of the outer and inner mass). To the best of our knowledge, and although such weakly nonlocal solitary waves have been studied extensively in a series of examples in physical sciences and engineering [35], this is only the second example of the reporting of such a nanopteronic solution in granular systems (and the first where such waves are obtained as exact solutions). The potential observation of such solutions in granular systems has been earlier suggested based on the numerical observations of [29], while this possibility has been proposed theoretically a decade ago for FPU lattices in the work of [36]. This motivates us to further examine the problem using the methodology of [27]. As a result of this study we illustrate that it is possible in fact to produce nanoptera with oscillating tails on both ends of the principal pulse. These results pave the way for a previously unexplored class of solutions in these “mass-in-mass” systems and render them especially intriguing candidates for experimental investigations.

Our presentation is structured as follows. In Section II, we offer the basic setup and the corresponding theoretical model. In Section III, we provide the analytical approach that captures the typical (and systematic) decay of a primary pulse in the “mass-in-mass” (hereafter abbreviated as MiM) system. In Section IV, we test these predictions numerically, obtaining good agreement with the analytical predictions, but also shedding light on how a nanopteronic solution can be seen to spontaneously emerge. In Section V, we propose a different analytical-numerical approach for capturing such solutions and offer a proof-of-principle confirmation of their existence (with tails on both sides of the principal pulse). Finally, in Section VI, we summarize our results and present our conclusions, as well as a number of directions for future study. Lastly, in the appendix we provide some technical details about the form of the traveling wave in the homogeneous granular chain that are used in our theoretical approach for capturing the decay of the primary pulse in the MiM setting.

II. PHYSICAL MODEL

In the present study we consider the uncompressed, one-dimensional, locally resonant granular crystal composed of hollow elastic spheres in contact, containing linear resonators, as this is illustrated in Figure 1. According to [37], the contact interaction of two hollow spheres depends strongly on the thickness of the spherical shells. However, for relatively thick spherical shells, the interaction contact follows the Hertzian contact law [1].

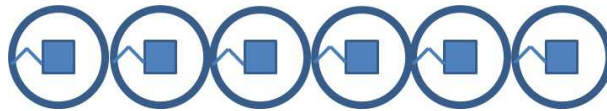


FIG. 1: Scheme of the model under consideration

The governing equations of motion can then be written as follows,

$$\begin{aligned} M_i \frac{d^2 U_i}{dt^2} &= \left(\frac{4}{3}\right) E^* \sqrt{R} \left[(U_{i-1} - U_i)_+^{3/2} - (U_i - U_{i+1})_+^{3/2} \right] + k(u_i - U_i), \quad \forall i, i \in N \\ m_i \frac{d^2 u_i}{dt^2} &= -k(u_i - U_i). \end{aligned} \quad (1)$$

Here U_i is the displacement of the i^{th} sphere, while u_i is the displacement of the small mass, linearly coupled attachment inside the i^{th} sphere, r_i is the radius of the sphere, M_i is the mass of the sphere; and $E^* = E/2(1 - \mu^2)$; E is the elastic (Young’s) modulus and μ is the Poisson’s ratio of the sphere. We note that the interaction force between the neighboring elements is given by $F = (4/3) E^* \sqrt{\frac{R_i}{2}} \Delta^{3/2}$, where r_i is bead radius (assumed implicitly to be uniform in the above expression i.e., independent of i) and Δ is their relative displacement. Moreover, the (+) subscripts in (1) and (3) indicate that only non-negative values of the expressions in parentheses are considered, i.e., the interaction is tensionless. We should also mention in passing that a mathematically similar system with (isolated) external resonators (a so-called mass-with-mass setting) has recently been proposed in [38]. It is noteworthy that though the mathematical equivalence of these two settings, their experimental realizations are quite different.

The system nondimensionalization is performed as follows

$$X_i = \frac{U_i}{r_i}; \quad x_i = \frac{u_i}{r_i}; \quad \tau = \left[\frac{E^*}{\sqrt{2\pi}r_i^2\rho} \right]^{1/2} t; \quad \tilde{\kappa} = \frac{3\sqrt{2}k}{4R_i E^*}; \quad \nu = \frac{m_i}{M_i} = \frac{m}{M}. \quad (2)$$

It is important to note that in the present study we assume (with one caveat to be explained below) that the outer and inner masses are uniform all through the chain (i.e. $r_i = r, M_i = M, m_i = m$).

Substituting (2) into (1) we end up with the following, non-dimensional set of equations governing the system dynamics

$$\begin{aligned} X_{i,\tau\tau} &= \left[(X_{i-1} - X_i)_+^{3/2} - (X_i - X_{i+1})_+^{3/2} \right] + \tilde{\kappa} (x_i - X_i) \\ \nu x_{i,\tau\tau} &= -\tilde{\kappa} (x_i - X_i). \end{aligned} \quad (3)$$

To make the further analysis of (3) somewhat simpler it is convenient to introduce the coordinates of relative displacements (i.e., strains) for both outer and inner masses,

$$\Delta_i = X_i - X_{i+1} \quad (4)$$

$$d_i = x_i - x_{i+1}. \quad (5)$$

Substituting (4) and (5) into (3) we obtain the following set of equations,

$$\begin{aligned} \Delta_{i,\tau\tau} &= \Delta_{(i-1),+}^{3/2} - 2\Delta_{(i),+}^{3/2} + \Delta_{(i+1),+}^{3/2} + \tilde{\kappa} (d_i - \Delta_i) \\ \nu d_{i,\tau\tau} &= -\tilde{\kappa} (d_i - \Delta_i). \end{aligned} \quad (6)$$

The goal of the present study is to examine the wave propagation along the contacts of the outer masses (which contribute to highly nonlinear dynamics) in the presence of the internal mass attachments. We assume that the coupling between the internal mass and the outer sphere is linear and weak such that $\tilde{\kappa}$ treated as a small system parameter $\tilde{\kappa} = \varepsilon$. We anticipate that as the primary pulse propagates down the chain, it is possible for it to “transfer” energy to the internal, linear attachments, storing it in the form of potential energy and thus depriving the original pulse from its initial kinetic energy. This, in turn, is expected to yield a decay of the amplitude of the primary pulse, which we now consider in three distinct asymptotic limits, namely: (1) $\nu \ll 1$, (2) $\nu = O(1)$ and (3) $\nu \gg 1$.

Nevertheless, as we will show below, the phenomenology is not exhausted in the (very accurately captured through our theoretical approach) pulse decay. In addition to it, we will illustrate the ability of the system to spontaneously rearrange its propagating waveform into the shape of a nanopterion i.e., a weakly nonlocal solitary wave with a non-vanishing tail that we subsequently study separately.

III. ANALYTICAL APPROXIMATION OF THE PRIMARY PULSE TRANSMISSION

We start our analysis by noting that due to the linear coupling between outer and inner masses, one can readily express the response of the relative displacement corresponding to inner masses by means of the relative displacement of the heavy spheres. Thus, using the well-known theory of Green’s functions one derives the solution for the relative displacement of the attachments in the following form,

$$\begin{aligned} d_i(t) &= \varepsilon\nu^{-1} \int_{-\infty}^t g(t|\tau) \Delta_i(\tau) d\tau = \omega_0 \int_{-\infty}^t \sin(\omega_0(t-\tau)) \Delta_i(\tau) d\tau \\ g(t|\tau) &= \omega_0^{-1} \sin(\omega_0(t-\tau)) \end{aligned} \quad (7)$$

where $\omega_0^2 = \varepsilon\nu^{-1}$, while $g(t|\tau)$ is a Green’s function of the undamped linear oscillator. Substituting (7) into the equation for the $\Delta_i(t)$, we obtain,

$$\begin{aligned} \Delta_{i,tt} &= \Delta_{(i-1),+}^{3/2} - 2\Delta_{(i),+}^{3/2} + \Delta_{(i+1),+}^{3/2} + \varepsilon Q(\Delta_i, t) \\ Q(\Delta_i, t) &= \left(\omega_0 \int_{-\infty}^t \sin(\omega_0(t-\tau)) \Delta_i(\tau) d\tau - \Delta_i(\tau) \right). \end{aligned} \quad (8)$$

Further analysis of the system is based on the recently proposed analytical procedure of [31], considering the evolution of the primary pulse along with its propagation through the granular chain subject to on-site perturbations. The main difference of the current system under consideration (10) from the previously considered ones examined in [31] is in the functional form of the perturbation term $Q(\Delta_i, t)$. To the best of the authors' knowledge, all the perturbed granular chains considered so far were autonomous, contrary to what is the case herein.

An additional significant difficulty observed in (8) is in the presence of the integral term in $Q(\Delta_i, t)$. This means that in order to derive the analytical approximation for the spatial evolution of the primary pulse, one has to cope with an integro-differential equation (8) rather than the ordinary differential equations analyzed previously.

In this section we develop an analytical procedure depicting the evolution of the amplitude of the propagating primary pulse interacting with the linear and weak, $\tilde{\kappa} = \varepsilon$, local resonators. The proposed analytical approach is based on the assumption that the functional form of the primary pulse can be approximated by the well-known solitary wave solution, originally developed in [2] - see also [1] for review derived for the unperturbed case of $\kappa = 0$ which has a well known form of Nesterenko soliton derived in the continuum limit [1]. This takes the following form:

$$\Delta_i^s(\tau) = S^s(\tau - i) = \begin{cases} B \cos^4(\alpha(\tau - i)), & \tau \in [i - \frac{\pi}{2\alpha}, i + \frac{\pi}{2\alpha}] \\ 0, & \text{otherwise} \end{cases} \quad (9)$$

where B and α corresponds to the amplitude and width of the normalized, solitary wave solution of unit phase shift ($T=1$). These parameters have been calculated in such a way that the amplitude and the areas of exact and approximate solitary wave profiles match.

In fact the parameters α and B can be considered as universal (see the Appendix for details) and thus, the general solitary wave solution propagating through the i^{th} contact element of the unperturbed chain can be written as

$$S_i(\tau) = AS^s(A^{1/4}\tau - i) \quad (10)$$

where A is the ratio between the amplitude of the arbitrary, solitary wave profile and the normalized on $S^s(0)$, and i is an index of the contact between the i^{th} and $(i+1)^{\text{th}}$ elements of the granular chain.

A. Limit of small mass attachments $\nu \ll 1$

Let us start with the analysis of a primary pulse transmission assuming the first asymptotic limit, $\tilde{\kappa} = \varepsilon$. In this limit, ω_0 is of $O(1)$.

Following the principal steps of [31, 39], for each contact in the chain we assign the local, semi-infinite time frame $t_i = t - T_{si}$, such that $t_i = 0$ corresponds to the exact time point when the i^{th} contact reaches the first peak of the primary pulse of the propagating disturbance. We assume that for the considered time interval $t_i \in (-\infty, 0]$, the primary pulse response recorded on the $(i-1)^{\text{th}}$, i^{th} , $(i+1)^{\text{th}}$ contacts exhibits a solitary-like behavior and thus can be approximated as, $\Delta_p(t) = A_p \tilde{S}(A_p^{1/4}t_i + i - p) + o(\varepsilon)$, where $p = i-1, i, i+1$, $T_{si} = T_{s(i-1)} + A_{i-1}^{-1/4} + \psi_0$ and ψ_0 controls the initial phase. Here, we set $\psi_0 = 0$. For the variable \tilde{S} , we will again use the subscript i to denote its value at the i^{th} spatial site.

Next, plugging the above *ansatz* into the integro-differential equation (8) we obtain,

$$B^{-1/2}A_i^{3/2}\tilde{S}''_i = A_{i-1}^{3/2}\tilde{S}_{i-1}^{3/2} - 2A_i^{3/2}\tilde{S}_i^{3/2} + A_{i+1}^{3/2}\tilde{S}_{i+1}^{3/2} + B^{-1/2}\varepsilon A_i \left(\omega_0 \int_{-\infty}^{t_i} \sin(\omega_0(t_i - \tau)) \tilde{S}_i(A_i^{1/4}\tau) d\tau - \tilde{S}_i \right) + o(\varepsilon). \quad (11)$$

Here the notion $\tilde{S}_p = \tilde{S}(A_p^{1/4}t_i + i - p) = \begin{cases} \cos^4(\alpha(A_p^{1/4}t_i + i - p)), & t_i \in \left[-\frac{\pi}{2\alpha A_p^{1/4}}, 0\right] \\ 0, & t_i \in \left[-\infty, -\frac{\pi}{2\alpha A_p^{1/4}}\right] \end{cases}$, where $p = i-1, i, i+1$,

has been used for the sake of brevity. It is important to note that (11) is a valid approximation for a solitary like behavior in the time interval $(-\infty, 0)$.

The above *ansatz* has accounted for the time dependence in the problem and has, in turn converted it into a *discrete* problem for identifying the elements of the sequence $\{A_i\}$ which essentially depict the evolution of the primary pulse along with its propagation through the perturbed granular chain using an iterative procedure.

The next step in the approximation is a direct integration of (11) in the local time interval $(-\infty, 0]$, leading to the following expression,

$$0 = A_{i-1}^{3/2} \int_{-\infty}^0 \tilde{S}^{3/2} \left(A_{i-1}^{1/4} t_i + 1 \right) dt_i - 2A_i^{3/2} \int_{-\infty}^0 \tilde{S}^{3/2} \left(A_{i-1}^{1/4} t_i \right) dt_i + A_{i+1}^{3/2} \int_{-\infty}^0 \tilde{S}^{3/2} \left(A_{i-1}^{1/4} t_i - 1 \right) dt_i \\ + B^{-1/2} \varepsilon A_i \left[\omega_0 \int_{-\infty}^0 \left(\int_{-\infty}^{t_i} \sin(\omega_0(t_i - \tau)) \tilde{S} \left(A_i^{1/4} \tau \right) d\tau \right) dt_i - \int_{-\infty}^0 \tilde{S} \left(A_i^{1/4} t_i \right) dt_i \right] + o(\varepsilon) \quad (12)$$

$$t_i \in (-\infty, 0].$$

It is important to note that the inertia term of (11) vanishes in (12) right after the integration in the specified time interval. This is precisely the reason for the choice of T_{S_i} as the time of the first peak of the primary pulse where the first derivative vanishes (*i.e.*, $\dot{\Delta}_i(t_i)|_{t_i=0} = 0$).

By a proper scaling of time in the first, second, third and fifth terms of (12) (*i.e.* $t_i \rightarrow A_{i-1} t_i$ (first term), $t_i \rightarrow A_i t_i$, (second and fifth terms), $t_i \rightarrow A_{i+1} t_i$ (third term)) one obtains the following simplification,

$$0 = A_{i-1}^{5/4} f_1 - 2A_i^{5/4} f_2 + A_{i+1}^{5/4} f_3 + B^{-1/2} \varepsilon \left(A_i \omega_0 \int_{-\infty}^0 \left(\int_{-\infty}^{t_i} \sin(\omega_0(t_i - \tau)) \tilde{S} \left(A_i^{1/4} \tau \right) d\tau \right) dt_i - A_i^{3/4} g_{1000} \right) + o(\varepsilon) \quad (13)$$

where $f_1 = \int_{-\infty}^0 \tilde{S}^{3/2}(t_i + 1) dt_i = 1.4568$, $f_2 = \int_{-\infty}^0 \tilde{S}^{3/2}(t_i) dt_i = 0.7615$, $f_3 = \int_{-\infty}^0 \tilde{S}^{3/2}(t_i - 1) dt_i = 0.0663$ and $g_{1000} = \int_{-\infty}^0 \tilde{S}(t_i) dt_i = 0.9138$. These integrations have been carried out by utilizing the approximate form of the travelling solitary wave solution; see the Appendix for details.

Here we make a note that the developed analytical procedure applied on (12) ultimately connects A_{i-1} with A_i and A_{i+1} . Thus, it is not sufficient for extracting the sequence of A_i 's and necessitates additional assumptions. A reasonable one such is that the variation of the amplitude of the primary pulse profile propagating from contact to contact is bounded by the order of applied perturbation, namely

$$A_{i+1} = A_i + \varepsilon \Delta + o(\varepsilon). \quad (14)$$

Moreover, we identify an additional small parameter in (13),

$$\mu = f_3/f_1 \ll 1, \quad \mu \ll f_2/f_1. \quad (15)$$

Thus, maintaining the first term stemming from the right hand side of (14) and neglecting terms $\propto \varepsilon \mu$, while preserving only terms $\propto \varepsilon$ and $\propto \mu$, we have that:

$$0 = A_{i-1}^{5/4} - 2A_i^{5/4} \left(f_2/f_1 \right) + A_i^{5/4} \mu \\ + B^{-1/2} \frac{\varepsilon}{f_1} \left(A_i \omega_0 \int_{-\infty}^0 \left(\int_{-\infty}^{t_i} \sin(\omega_0(t_i - \tau)) \tilde{S} \left(A_i^{1/4} \tau \right) d\tau \right) dt_i - A_i^{3/4} g_{1000} \right) + O(\varepsilon \mu) + o(\varepsilon). \quad (16)$$

At this level of approximation, (16) defines a nonlinear, one-dimensional map ($A_{i-1} \rightarrow A_i$), which can not be explicitly solved. Equation (16) is solved iteratively at each step determining the resulting amplitude of the primary pulse $\{A_i\}$.

The system (16) can be rewritten in a more compact form

$$A_i^{5/4} \left(-2 \frac{f_2}{f_1} + \mu \right) + B^{-1/2} \frac{\varepsilon}{f_1} \left(A_i I(\omega_0, A_i) - A_i^{3/4} g_{1000} \right) + A_{i-1}^{5/4} = 0 \quad (17)$$

where $I(\omega_0, A_i) = \omega_0 \int_{-\infty}^0 \left(\int_{-\infty}^{t_i} \sin(\omega_0(t_i - \tau)) \tilde{S} \left(A_i^{1/4} \tau \right) d\tau \right) dt_i = \omega_0 A_i^{-1/2} \int_{-\infty}^0 \left(\int_{-\infty}^{\xi} \sin(\omega_0 A_i^{-1/4}(\xi - \phi)) \tilde{S}(\phi) d\phi \right) d\xi$.

The direct integration of (17), yields the explicit nonlinear map as following:

$$A_i^{5/4} \left(-2\frac{f_2}{f_1} + \mu \right) + B^{-1/2} \frac{\varepsilon}{f_1} \left(A_i^{3/4} \left(\frac{3\pi}{16\alpha} - g_{1000} \right) - \frac{24\alpha^4 A_i^2 \sin \left(\frac{\omega_0 \pi}{2\alpha A_i^{1/4}} \right)}{\omega_0 \left(\omega_0^4 - 20\omega_0^2 \alpha^2 A_i^{1/2} + 64\alpha^4 A_i \right)} \right) + A_{i-1}^{5/4} = 0. \quad (18)$$

Fortunately, for the case of uniformly perturbed chains (i.e., ε and ω_0 remain constants all through the chain), the expression (18) can be homogenized.

Thus, performing the transformation $A_i^{5/4} = D_i$ leads to

$$0 = f_1 D_{i-1} - 2f_2 D_i + f_3 D_{i+1} + \varepsilon B^{-1/2} D_i^{3/5} \left[\left(\frac{3\pi}{16\alpha} - g_{1000} \right) - \frac{24\alpha^4 D_i \sin \left(\frac{\omega_0 \pi}{2\alpha D_i^{1/5}} \right)}{\omega_0 \left(\omega_0^4 - 20\omega_0^2 \alpha^2 D_i^{2/5} + 64\alpha^4 D_i^{4/5} \right)} \right]. \quad (19)$$

A long-wave approximation then yields the following transformation:

$$D_i = D, \quad D_{i-1} = D - hD' + O(h^2), \quad D_{i+1} = D + hD' + O(h^2). \quad (20)$$

After the substitution, we obtain the ODE of the first order

$$hD' = \frac{\varepsilon B^{-1/2} D^{3/5}}{f_3 - f_1} \left[\frac{24\alpha^4 D \sin \left(\frac{\omega_0 \pi}{2\alpha D^{1/5}} \right)}{\omega_0 \left(\omega_0^4 - 20\omega_0^2 \alpha^2 D^{2/5} + 64\alpha^4 D^{4/5} \right)} - \left(\frac{3\pi}{16\alpha} - g_{1000} \right) \right]. \quad (21)$$

It is obvious that, in the normalized system under investigation $h = 1$, and thus, the system is rewritten as

$$D' = \frac{\varepsilon B^{-1/2} D^{3/5}}{f_3 - f_1} \left[\frac{24\alpha^4 D \sin \left(\frac{\omega_0 \pi}{2\alpha D^{1/5}} \right)}{\omega_0 \left(\omega_0^4 - 20\omega_0^2 \alpha^2 D^{2/5} + 64\alpha^4 D^{4/5} \right)} - \left(\frac{3\pi}{16\alpha} - g_{1000} \right) \right]. \quad (22)$$

It is worthwhile to note that after computing the drop in the response recorded on the contacts of the outer spheres, one can recover explicitly the primary response of the internal resonators. Thus performing the integration of (7) one arrives at the following form:

$$d_i(t_i) = \begin{cases} 0, & t_i \in \left(-\infty, -A_i^{-1/4} \frac{\pi}{2\alpha} \right] \\ C_1 \cos^4 \left(\alpha A_i^{1/4} t_i \right) + C_2 \left(1 - \cos \left(\omega_0 t_i + \frac{\pi \omega_0}{2\alpha A_i^{1/4}} \right) \right) + C_3 \cos^2 \left(\alpha A_i^{1/4} t_i \right), & t_i \in \left[-A_i^{-1/4} \frac{\pi}{2\alpha}, A_i^{-1/4} \frac{\pi}{2\alpha} \right] \\ U \sin \left(\omega_0 t_i \right) \sin \left(\frac{\pi \omega_0}{2\alpha A_i^{1/4}} \right), & t_i \in \left[A_i^{-1/4} \frac{\pi}{2\alpha}, +\infty \right) \end{cases} \quad (23)$$

where $C_1 = \frac{-4A_i B \omega_0^2 \left(\alpha^2 A_i^{1/2} - \frac{\omega_0^2}{4} \right)}{K}$, $C_2 = \frac{24\alpha^4 A_i^2 B}{K}$, $C_3 = \frac{-12\alpha^2 \omega_0^2 A_i^{3/2} B}{K}$, $U = \frac{48A_i^2 \alpha^4 B}{K}$ and $K = \omega_0^4 - 20\omega_0^2 \alpha^2 A_i^{1/2} + 64\alpha^4 A_i$. Nevertheless, it should be highlighted that the above obtained quadrature solution provides a rather uncontrolled approximation, as there is no small parameter for this expansion (notice that h has been set to unity). On the other hand, that is an approximation that occasionally works unexpectedly well in the context of granular crystals [1].

B. Comparable masses $\nu = O(1)$

In the present subsection we analyze the evolution of the primary pulse in the case of the internal mass being comparable to that of the outer sphere. Though this case can be directly addressed by the already developed approximation (18), the main purpose of the present subsection is to show that this approximation can be simplified even more in the case of $\nu = O(1)$.

Starting from the construction of the map, we have

$$A_i^{5/4} \left(-2\frac{f_2}{f_1} + \mu \right) + B^{-1/2} \frac{\varepsilon}{f_1} \left(A_i^{3/4} \left(\frac{3\pi}{16\alpha} - g_{1000} \right) - \frac{24\alpha^4 A_i^2 \sin \left(\frac{\omega_0 \pi}{2\alpha A_i^{1/4}} \right)}{\omega_0 \left(\omega_0^4 - 20\omega_0^2 \alpha^2 A_i^{1/2} + 64\alpha^4 A_i \right)} \right) + A_{i-1}^{5/4} = 0. \quad (24)$$

Accounting for $\nu = O(1)$ and expanding the term containing the sin in Taylor series (with respect to ϵ) up to the first order, yields the following simplification of the nonlinear map (24),

$$0 = A_{i-1}^{5/4} - 2A_i^{5/4} \frac{f_2}{f_1} + A_i^{5/4} \mu - B^{-1/2} \frac{\epsilon}{f_1} \left(A_i^{3/4} g_{1000} \right). \quad (25)$$

As the local oscillator acts now purely on the outer shell of our granular hollow spheres, the evolution of the primary pulse becomes tantamount to that of the granular chain, mounted on a linear elastic foundation, a case examined in [31]. Again, arguing exactly as above (i.e. (20)–(22)) the appropriate long wave approximation can be explicitly derived for the nonlinear map (25). Here we would like to emphasize that unlike the previous case, in the case of the heavy internal masses the expression for the long wave approximation depicting the spatial evolution of the primary pulse, takes the following explicit form:

$$A = \left\{ A_0^{1/2} - \frac{2}{5} \frac{B^{-1/2} \epsilon g_{1000} \xi}{f_1} \right\}^2 \quad (26)$$

where A_0 is the amplitude of the solitary wave pulse impinging on the perturbed part of the chain and ξ is the continuum variable associated with the site i in the long wavelength limit developed in [31].

C. Limit of the heavy internal masses $\nu \gg 1$

In the present subsection we consider the case of $\nu \gg 1$. We again start from the rescaled system (3). Keeping in mind that ϵ is a small parameter and accounting for a high mass mismatch ($\nu \gg 1$), we can rewrite the system as

$$\begin{aligned} X_{i,\tau\tau} &= \left[(X_{i-1} - X_i)_+^{3/2} - (X_i - X_{i+1})_+^{3/2} \right] + \epsilon (x_i - X_i) \\ x_{i,\tau\tau} &= 0 \end{aligned} \quad (27)$$

by letting $\epsilon/\nu \rightarrow 0$. This, coupled with the vanishing initial conditions on the internal oscillators, yields the immediate reduction,

$$X_{i,\tau\tau} = \left[(X_{i-1} - X_i)_+^{3/2} - (X_i - X_{i+1})_+^{3/2} \right] - \epsilon X_i \quad (28)$$

which once again leads to the dynamics of a homogeneous granular chain mounted on an elastic foundation.

In fact in the case of hard excitation, (i.e., for $X_i = O(1)$) the response of (28) can be described by a nonlinear mapping procedure (25) and (26) depicting the modulation of solitary like pulses. However, for the case of the low amplitude excitations (i.e., for $X_i = O(\epsilon^2)$) system (28) can be immediately rescaled, ($X_i = \epsilon^2 \bar{x}_i, \bar{t} = \sqrt{\epsilon} \tau$) yielding

$$\bar{x}_i'' + \bar{x}_i = \left[(\bar{x}_{i-1} - \bar{x}_i)_+^{3/2} - (\bar{x}_i - \bar{x}_{i+1})_+^{3/2} \right]. \quad (29)$$

This system has been recently considered in [28, 29]. There, it was shown analytically and numerically that this system supports various periodic solutions, ranging from spatially periodic standing and traveling waves up to strongly localized ones (i.e. standing and moving breathers).

IV. NUMERICAL SIMULATIONS

A. Model Setup

We now consider detailed numerical simulations of the model. The goal is twofold, to examine the predictions of the analytical approximations based on the nonlinear map approach of the previous section and to reveal additional features of the emerging coherent structures. Regarding the first goal, it is important to emphasize that the analytical scheme of the nonlinear map, assumes that the propagating primary pulse has a waveform in the shape of a Nesterenko soliton [1, 2]. Therefore, to assure that the primary pulse impinging on the perturbed part of the chain (the MiM lattice) has already assumed a solitary waveform, we select the initial part of the chain to be composed of typically 39 uniform, hollow spheres (cf. Figure 2) and we consider a velocity impulsive excitation.

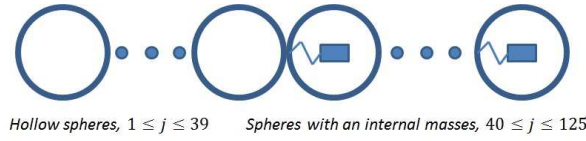


FIG. 2: Scheme of the model which is used in numerical simulations.

Thus, the dynamical model under consideration in the present numerical study reads:

$$\begin{aligned}
 X_{i,\tau\tau} &= (1 - \delta_{1,i}) (X_{i-1} - X_i)_+^{3/2} - (X_i - X_{i+1})_+^{3/2}, & 2 \leq i < 41 \\
 X_{i,\tau\tau} &= (X_{i-1} - X_i)_+^{3/2} - (1 - \delta_{i,125}) (X_i - X_{i+1})_+^{3/2} + \varepsilon (x_i - X_i), & 41 \leq i \leq 125 \\
 \nu x_{i,\tau\tau} &= -\varepsilon (x_i - X_i), & 41 \leq i \leq 125
 \end{aligned} \tag{30}$$

where $\delta_{1,i}$ and $\delta_{i,125}$ denote Kronecker symbols, and

$$\begin{aligned}
 X_{1,\tau}(0) &= \tilde{V}_0, X_1(0) = 0 \\
 X_i(0) &= X_{i,\tau}(0) = 0, & 2 \leq i \leq 125 \\
 x_i(0) &= x_{i,\tau}(0) = 0, & 41 \leq i \leq 125.
 \end{aligned} \tag{31}$$

From extensive simulations of this numerical configuration, we can distinguish the following three distinct cases:

Case (i): Weak coupling ($\varepsilon \ll 1$), light inner masses ($\nu = O(\varepsilon)$), initial excitation of the order of one ($\tilde{V}_0 = O(1)$).

Case (ii): Weak coupling ($\varepsilon \ll 1$), comparable or heavier inner masses ($\nu = O(1)$ or $\nu \geq 1$), initial excitation of the order of one ($\tilde{V}_0 = O(1)$).

Case (iii): Weak to moderate coupling ($\varepsilon = O(1)$), heavier inner masses ($\nu \geq 1$), weak initial excitation ($\tilde{V}_0 \ll 1$).

Intuitively, assuming the initial excitation to be of order $\tilde{V}_0 = O(1)$ the first two asymptotic cases correspond to the weak perturbation of the Nesterenko solitary wave. Clearly these two cases correspond to the hard excitation, as the strength of the initial excitation is much higher than that of the coupling term ε .

In fact for the case of a hard excitation (cases (i) and (ii)) it is rather convenient to perform an additional rescaling of (30). Thus introducing the new scales of time and displacements

$$\tilde{\tau} = \left(\tilde{V}_0^{1/5} \right) \tau, \quad \tilde{X}_i = \left(\tilde{V}_0^{-4/5} \right) X_i, \quad \tilde{x}_i = \left(\tilde{V}_0^{-4/5} \right) x_i \tag{32}$$

the rescaled system under consideration has a unit velocity kick (absorbed in the rescaling) and a renormalized $\tilde{\varepsilon} = \varepsilon \tilde{V}_0^{-2/5}$.

Accounting for the rescaling brought in (32), the limiting cases can be slightly reformulated as:

Case (i): $\varepsilon \ll 1$, $\nu = O(\varepsilon)$.

Case (ii): $\varepsilon \ll 1$, $\nu = O(1)$ or $\nu \geq 1$.

Case (iii): $\varepsilon \gg 1$, $\nu \geq 1$.

As it was pointed out in several works studying the dynamics of solitary waves impinging on the interface of the (mass mismatched) granular chains, in such cases there is a formation of a train of the transmitted and reflected pulses. In fact, in the framework of our study for the cases (i) and (ii), we adopt a certain asymptotic assumption, under which the perturbation induced by the local resonators is treated as a small parameter. This formally provides us with the right to assume that the primary pulse only slightly deviates from the unperturbed solution on each site (Nesterenko soliton). The third limiting case is rather different from cases (i) and (ii). In fact, unlike the first two cases which correspond to the evolution of solitary like pulses in the perturbed chain, case (iii) concerns the formation of moving breathers, previously studied in [28, 29]. In the rest of the paper all the numerical simulations corresponding to the asymptotic cases (i) and (ii) have been performed for the rescaled model, while when these related to the case (iii) have been performed for original one of (30).

B. Numerical Study of the Primary Pulse Transmission

A typical result of the system's evolution is presented in Figure 3 for $\tilde{\varepsilon} = 0.05$ and $\nu = 0.128$. Here, we plot the evolution of the relative displacement for numerous sites throughout the chain. These reveal a primary pulse response of the system, forming as a result of the impulsive excitation supplied to the left end of the chain. As it is clear

from the results of the figure, three main stages can be distinguished in the propagation of the primary pulse; (1) the undisturbed propagation of a solitary wave through the first part of the chain free of the chain (this propagation can be observed in Region 1) (2) the systematic drop in the amplitude of a single-hump primary pulse due to its interaction with the local resonators (Region 2) (3) formation of the complex (‘breathing’) modulated, multi-humped pulse patterns (Region 3). In the currently examined limit of $\tilde{\varepsilon} \ll 1$ and of $\nu = O(\tilde{\varepsilon})$, these findings can be considered as rather generic.

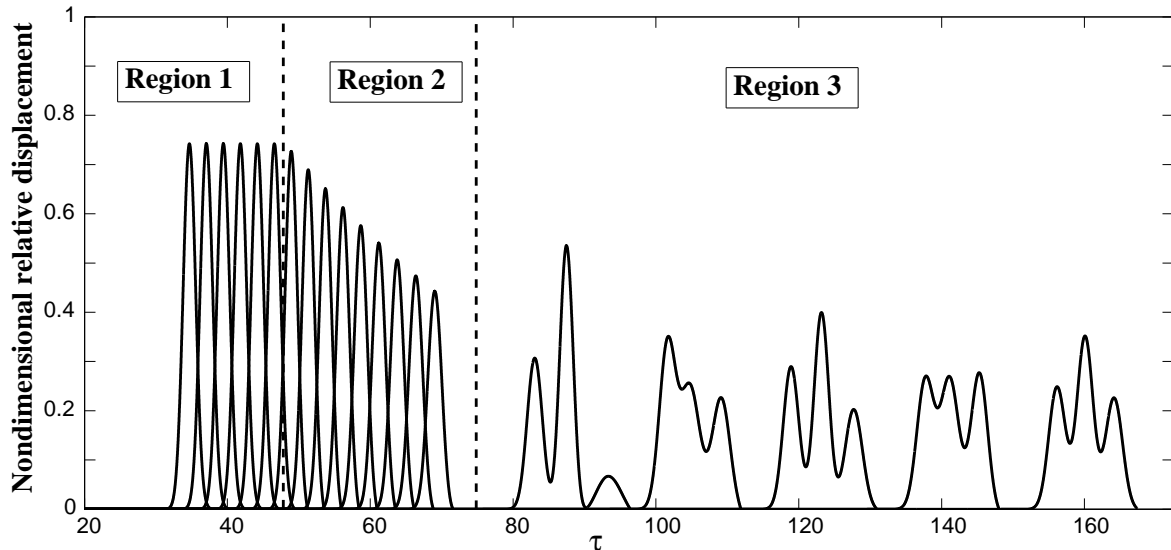


FIG. 3: Time histories of relative displacements for a number of different contacts in the chain, revealing the pulses recorded at the different contacts of the outer spheres. Parameters of the linear resonators: $\tilde{\varepsilon} = 0.05$, $\nu = 0.128$

A somewhat unexpected feature in the context of this model concerns the formation of the modulated wavetrains presented above in Figure 3, on which we now focus. To better visualize their mechanism of formation, we illustrate the gradual evolution of a secondary hump emerging along the chain in Figure 4, as the primary pulse decays. At the initial stage of the process the two humps (primary and secondary) are well separated, amplitude-wise. Alongside the decay of a single humped primary pulse, one observes the formation and gradual growth of the secondary (single-humped) pulse. On some specific contact of the chain the amplitude of the secondary hump exceeds the amplitude of the first one. Moreover, at some point the two humps (or more) merge into a modulated, multi-humped primary pulse (Region 3 of Figure 3). This modulation of the primary pulse constitutes a qualitatively new regime which obviously differs from the initial un-attenuated propagation of the solitary pulse (of Region 1) as well as from the monotonic decay of a single humped primary pulse (of Region 2).

Clearly, the analytical procedure developed in the previous section can only be valid in the Region 2 where the waveform of the primary pulse profile exhibits a single hump decaying due to the perturbation, yet preserving its solitary wave behavior, justifying the approximations of our analytical approach which we now test in detail.

C. Numerical Verifications of the Analytical Model

In this subsection we perform the detailed comparison between the analytical approximations of (18) and (26) predicting the evolution of the primary pulses (in Region 2) with the direct numerical simulations for the three main cases.

Case (i):

In Figures 5 and 6, we plot the evolution of the primary pulses in the second region for two fixed values ($\nu = 0.05$ and 0.25 ; similar results have been obtained for larger values e.g. for $\nu = 0.55$) of the internal masses, gradually increasing the value of the stiffness coefficient.

It is important to note that for the sake of better illustration of the global picture of a primary pulse transmission, in some figures we have also plotted the formation and evolution of the secondary humps.

Results of Figures 5 and 6 suggest that in the limit of small mass attachments and soft springs (i.e. $\tilde{\varepsilon} < 1$, $\nu \sim O(\tilde{\varepsilon})$) a strong rate of the decay of a single-humped primary pulse can be achieved. Moreover, as it is clear from the illustrated comparisons, the analytical predictions for the decay of a primary pulse given by (18) are found to be in very good

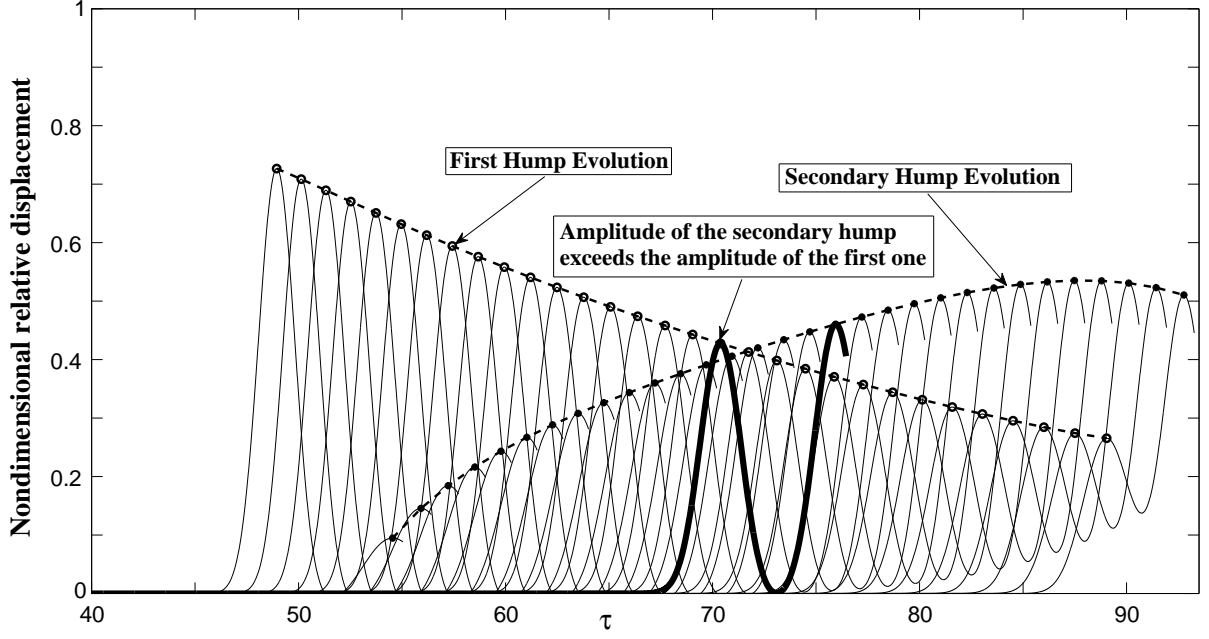


FIG. 4: Time histories (corresponding to the numerical simulation) revealing the evolution of the primary and secondary humps leading to the formation of the multi-humped primary pulses recorded on the different contacts of the outer spheres. Parameters of the linear resonators: $\tilde{\varepsilon} = 0.05$, $\nu = 0.128$. The evolution of the amplitudes of the primary and secondary humps is denoted by lines as a guide to the eye.

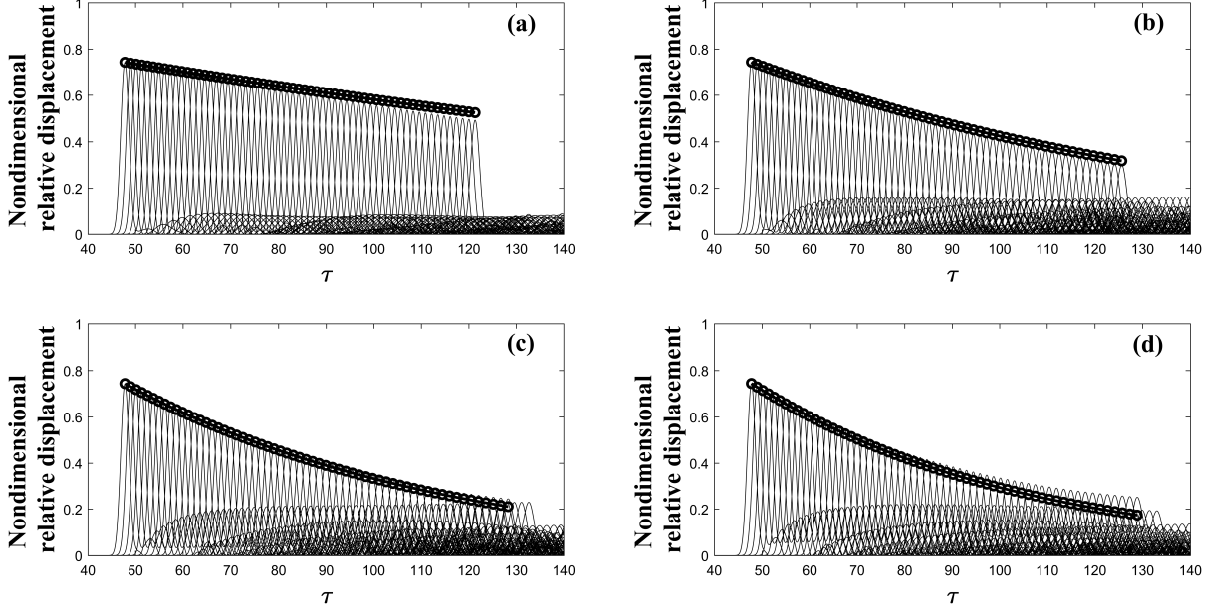


FIG. 5: Time histories of the evolution of the relative displacements showing the primary pulse in the second region, recorded on the first 60 contacts of the perturbed part of the chain. Results of numerical simulations are denoted with the solid lines; results of analytical approximation of (18) are denoted with the connected circles (o). System parameters: $\nu = 0.05$, (a) $\tilde{\varepsilon} = 0.01$, (b) $\tilde{\varepsilon} = 0.025$, (c) $\tilde{\varepsilon} = 0.04$ and (d) $\tilde{\varepsilon} = 0.05$.

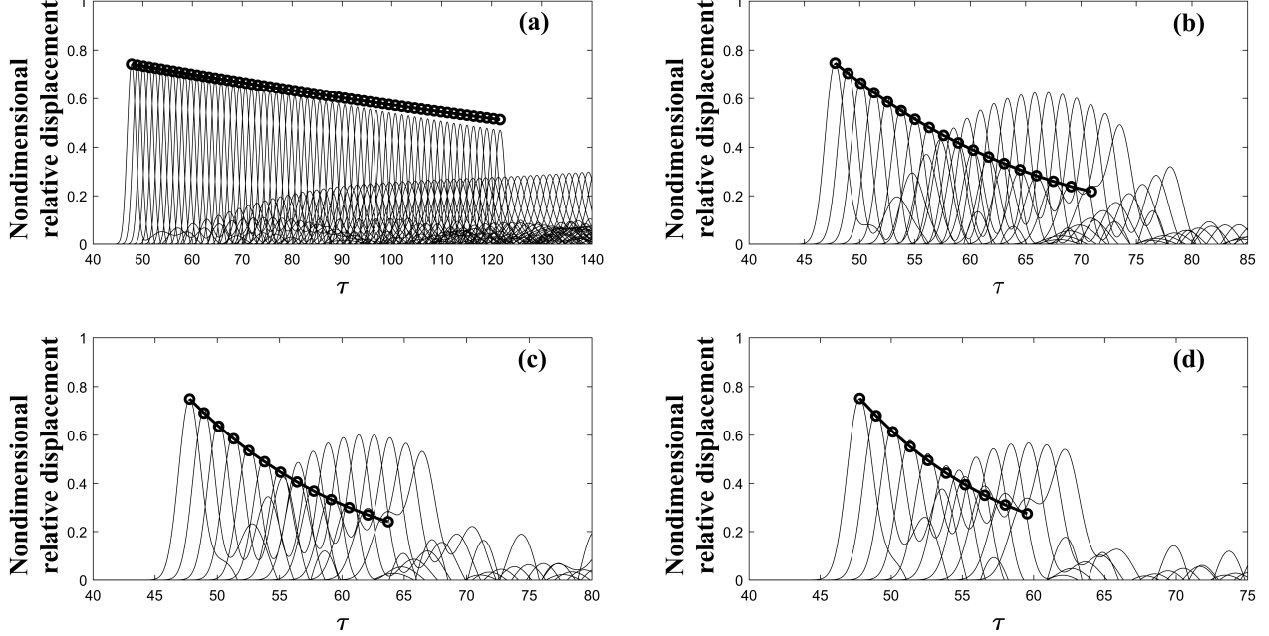


FIG. 6: Same as Figure 5 for system parameters: $\nu = 0.25$, (a) $\tilde{\varepsilon} = 0.01$, (b) $\tilde{\varepsilon} = 0.12$, (c) $\tilde{\varepsilon} = 0.18$ and (d) $\tilde{\varepsilon} = 0.25$.

correspondence with the results of the direct numerical simulations. It should be clear that in examining this decay, we are disregarding the formation of the secondary humps, which is an important feature in its own right that we will be concerned with below.

A more careful look at the results shows that on one hand by changing the value of the internal stiffness $\tilde{\varepsilon}$ (staying in the limit of a soft internal spring and small mass attachment $0 \leq \tilde{\varepsilon} \leq \nu \ll 1$), one can effectively control the rate of decay of a single-humped primary pulse. For example, as is shown in Figure 5 by fixing the value of $\nu = 0.05$ and varying the stiffness parameter in the range ($0 \leq \tilde{\varepsilon} \leq 0.05$) one can clearly observe the increasing rate of decay of the primary pulse. However, on the other hand for the higher values of the internal stiffness, the distortion of the primary pulse resulting in the formation of the secondary hump occurs much faster. In other words the number of contacts of the second region sustaining the evolution of a single-humped primary pulse significantly decreases with the growth in the stiffness parameter. Thus, the further increase in the value of an internal stiffness parameter may lead to a more rapid formation of the localized, modulated wave-packets (multi-humped primary pulses) which also signals the disappearance of the second region. Naturally, in that case the proposed analytical procedure cannot be applied.

As indicated above, when Region 2 exists and the pulse decays sufficiently slowly, the analytical approximation provides a highly accurate match to the decay of the principal pulse. Nevertheless, an additional question is whether the evolution of the inner masses is also captured by the approximation, as suggested e.g. by (23). Unfortunately, the answer to this question is in the negative, as clearly indicated in Figure 7. Although, the approximation captures the first stage of the passage of the primary pulse through the bead (and hence its internal attachment), it subsequently considerably overestimates, through its “rigid” traveling pulse assumption, the amplitude of the corresponding oscillation and even misses its exact frequency. Notice, in addition, that the true system dynamics in the tails can become considerably more complicated e.g. including the separation of the outer spheres and emergence of chaotic motions.

Case (ii):

From the discussion of Section III it is quite clear that for the cases of $\nu = O(1)$ or $\nu \gg 1$, for hard excitations the primary response of the system can be effectively approximated by a simplified model, namely by the uniform granular chain mounted on a linear elastic foundation. This type of the system has been studied analytically and numerically in [31]. In the same study it was shown that increasing the strength of elastic foundation (i.e. the value of the coefficient of stiffness) we increase the rate of the decay of the primary pulse. In the present study we demonstrate that the decay of the primary pulse in the case of the heavy mass attachments can be accurately approximated by the analysis of Section III.

To this end, we plot the drop in the amplitude of the primary pulse recorded on the first 10 contacts in Region 2 of the perturbed granular chain for the fixed value of the stiffness coefficient ($\tilde{\varepsilon} = 0.1$) and various values of the internal

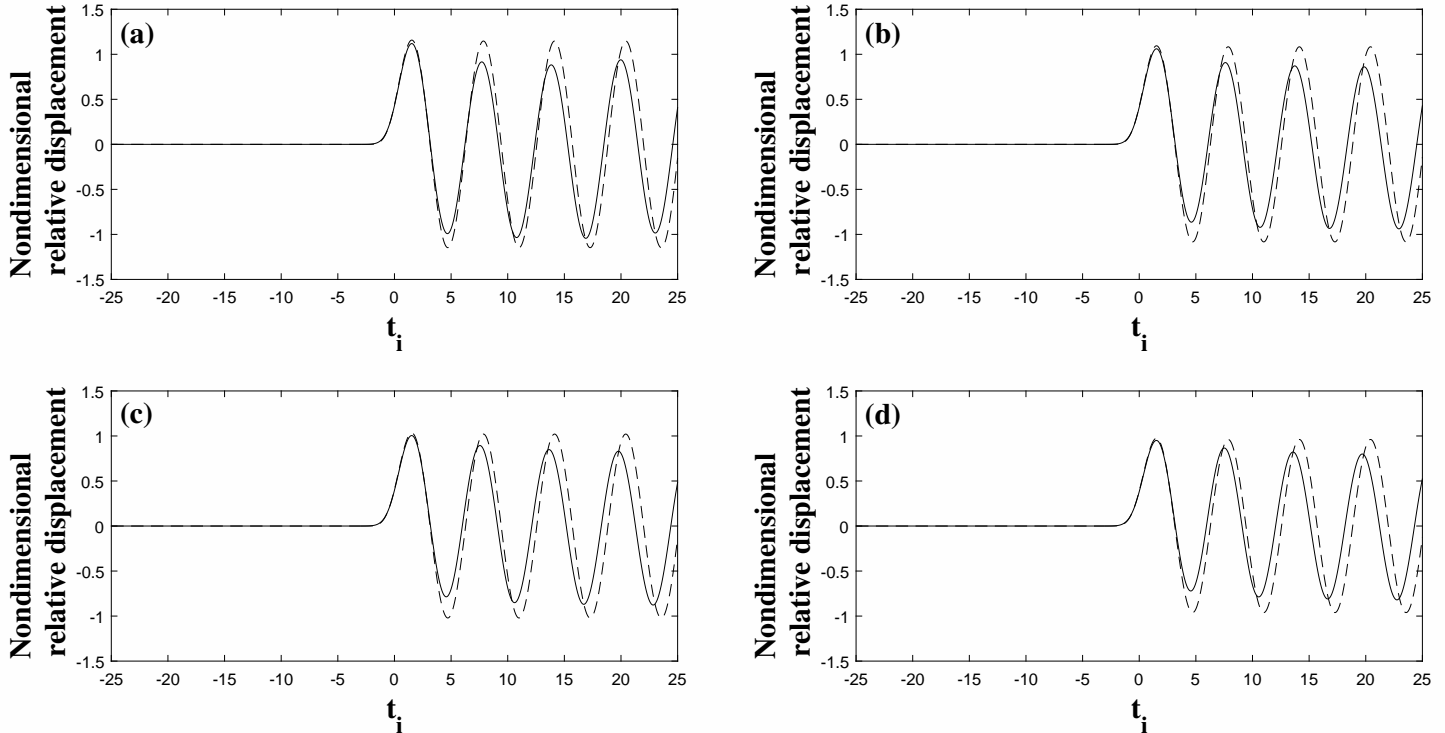


FIG. 7: Comparison of the response of the relative displacements of the internal attachments (d_i) as derived from (23) with the full direct numerical simulations. The response derived from (23) is denoted with the dashed line; results of direct numerical simulations are denoted with the solid line. System parameters: $\nu = 0.05$, $\tilde{\varepsilon} = 0.05$. (a) Response recorded on the 1st contact from the interface $d_1(t)$, (b) Response recorded on the 4th contact from the interface $d_4(t)$, (c) Response recorded on the 7th contact from the interface $d_7(t)$ and (d) Response recorded on the 10th contact from the interface $d_{10}(t)$.

masses ($\nu = 1, 3, 5, 10$) in Figure 8. The results suggest a very good correspondence of the analytical prediction of the drop with that of the numerical simulation.

Case (iii):

In Figure 9, we illustrate the formation of moving breathers for the low amplitude excitations and the case of heavy linear attachments. This feature serves to showcase the accordance of the full numerical simulation to the reduced order model (29), which supports such structures, as analyzed in the works of [28, 29]. Hence, we do not pursue this avenue further, but defer the interested reader to the detailed structures in such equations as presented in the above works.

D. Efficiency of Attenuation and the Formation of Robust Traveling Waves

To study the efficiency of the local resonators in inducing attenuation of the primary (single humped) pulses as they propagate through the perturbed part of the chain, one needs first to define a precise criterion.

Here, we have chosen to focus on the maximal velocity of the last element after its detaching from the chain. In each numerical run we set the initial velocity of the first element to unity (i.e. $V_0 = 1$) while the total number of the elements in the chain is fixed to $N = 125$ (here we note again that the first 39 elements contain no internal resonators while the rest elements of the chain incorporate, perfectly identical local resonators). In each numerical run we evaluate the maximal velocity of the last element $V_N(\tilde{\varepsilon}, \nu)$ after its complete detachment from the chain. It is worthwhile noting that the calculated data (i.e. $V_N(\tilde{\varepsilon}, \nu)$ for $0 < \tilde{\varepsilon}, \nu \leq 1$) is normalized with respect to the maximal velocity of the latter in the given range of the system parameters ($0 < \tilde{\varepsilon}, \nu \leq 1$) (See Figure 10).

From the observation of the results of Figure 10, it is clear that there is a certain tradeoff between the mass and the stiffness of the internal attachment leading to the best possible attenuation of the primary pulse. Moreover, a close look at the results of Figure 10 shows that the area of efficient attenuation is achieved for the relatively small values of

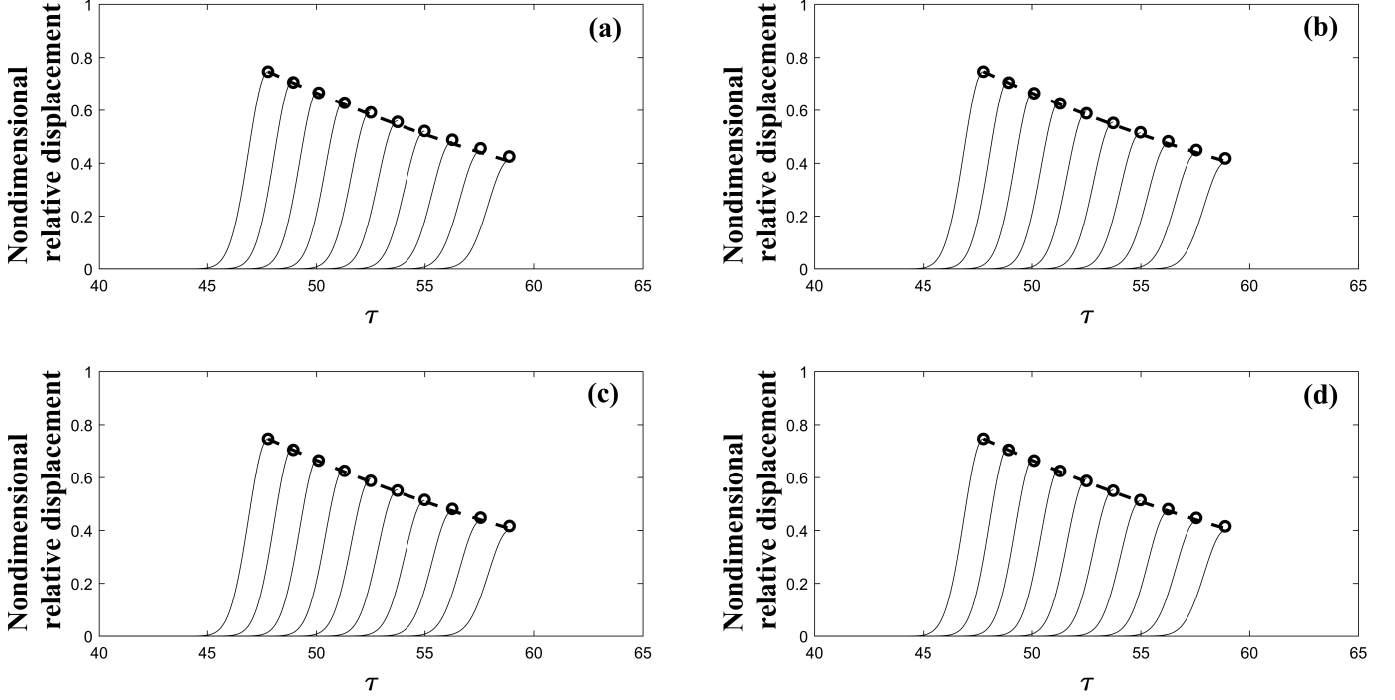


FIG. 8: Comparison of the analytical prediction and numerical simulation of the primary pulse amplitude decay on the outer spheres for $\tilde{\varepsilon} = 0.1$ (a) $\nu = 1$ (b) $\nu = 3$ (c) $\nu = 5$ (d) $\nu = 10$ in the non-dimensional relative displacement recorded on the contacts. The symbols denote the amplitudes of the primary pulse in terms of the relative displacement predicted by the map (18), while the dashed line shows the corresponding long wave approximation of (26). The bold black lines correspond to full

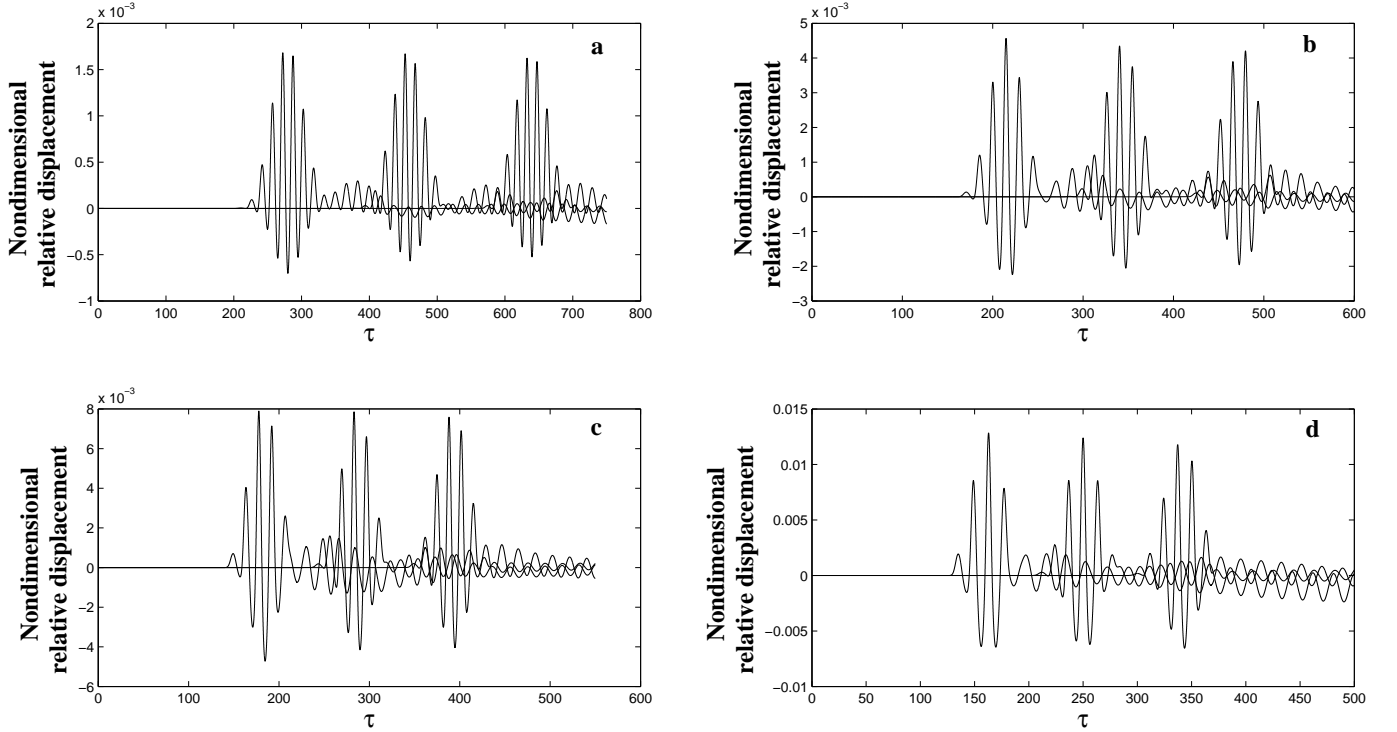


FIG. 9: The non-dimensional relative displacement recorded on the contacts from the direct numerical simulation of (6) $\varepsilon = 0.1$ (a) $\nu = 1$ (b) $\nu = 3$ (c) $\nu = 5$ (d) $\nu = 10$.

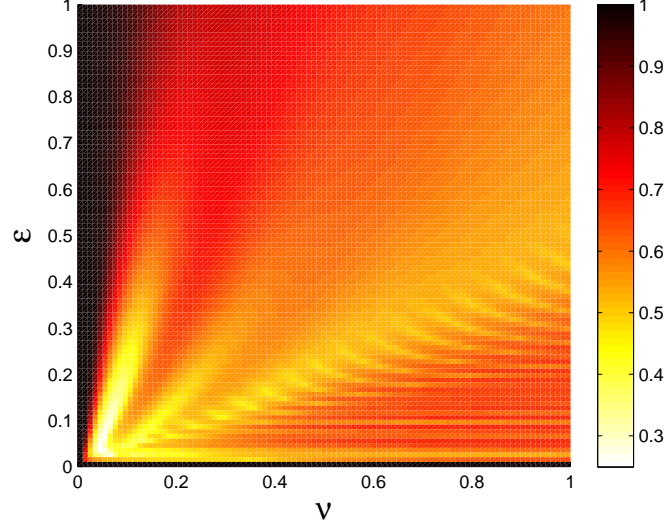


FIG. 10: Contour map of the attenuation diagnostic $V_N(\tilde{\epsilon}, \nu)$ in the range of $0 < \tilde{\epsilon}, \nu < 1$. The results correspond to full lattice numerical simulations.

the internal mass and stiffness coefficient. In particular, the very efficient attenuation is reached for $\tilde{\epsilon} \simeq 0.05, \nu \simeq 0.05$. In addition, one can observe the formation of the new regions corresponding to the case of the relatively heavy internal masses e.g. ($\tilde{\epsilon} \simeq 0.05, \nu \simeq 0.9$) leading to the efficient attenuation of the primary pulse.

Another very interesting observation made during the numerical study of the regimes corresponding to the third region is the formation of what appears to be stationary solitary like pulses of various shapes. In Figure 11, we plot an example of a single humped such pulse (left panel), as well as one of a double humped solitary wave (right panel), respectively which have been formed in the third region. Notice that in the latter, it is the hollow spheres that feature the double-humped response in time, while the inner attachment is still single-humped.

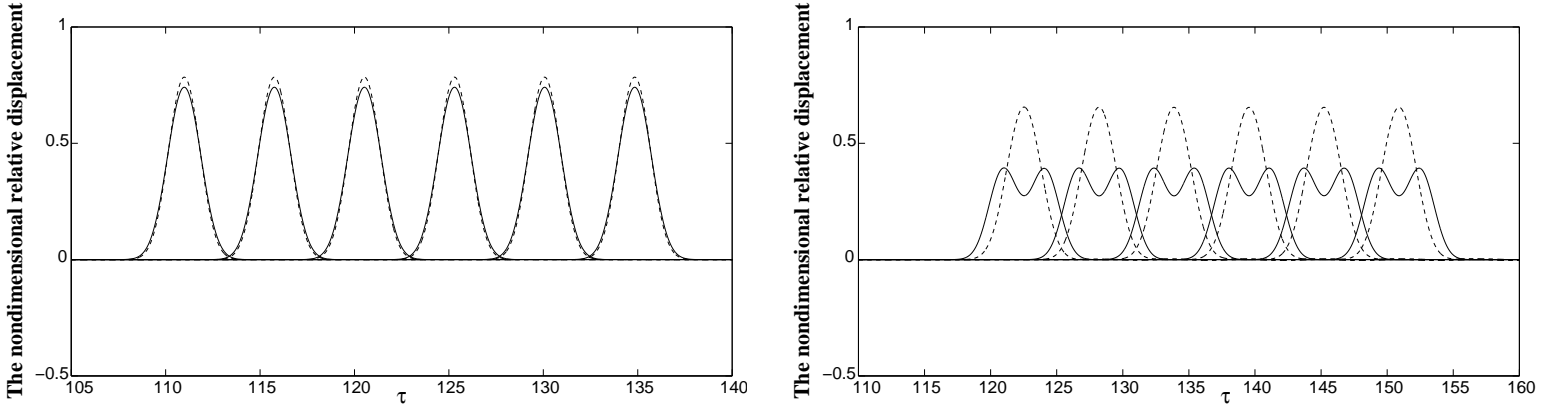


FIG. 11: Time histories from numerical simulations illustrating a single-humped solitary like pulse recorded on the six different contacts (92,94,96,98,100,102) in the third region (left panel). The system parameters are $\tilde{\epsilon} = 0.105$ and $\nu = 0.004$. A similar example but now for a double-humped solitary like pulse recorded on the six different contacts (92,94,96,98,100,102) in the third region is shown in the right panel. Here, the system parameters are $\tilde{\epsilon} = 0.105$ and $\nu = 0.10245$. In both cases, the solid line denotes the response of the outer masses, while the dashed line denotes the response of the inner masses.

These observations have led us to a more systematic study of such a response which is reflected in Figures 12 and 13. The former is for the case $\tilde{\epsilon} = 0.105, \nu = 0.10245$, while the latter for $\tilde{\epsilon} = 0.105, \nu = 0.004$. In these more detailed, larger scale runs, the wave is initialized at bead 1 while the interface is at bead 40 and all beads carry a local resonator thereafter. The space time plot in the top panel of Figure 12 (as well as in the left panel of Figure 13) already spells out the fundamental phenomenology. The initial excitation induces the formation of the traveling wave (notice that

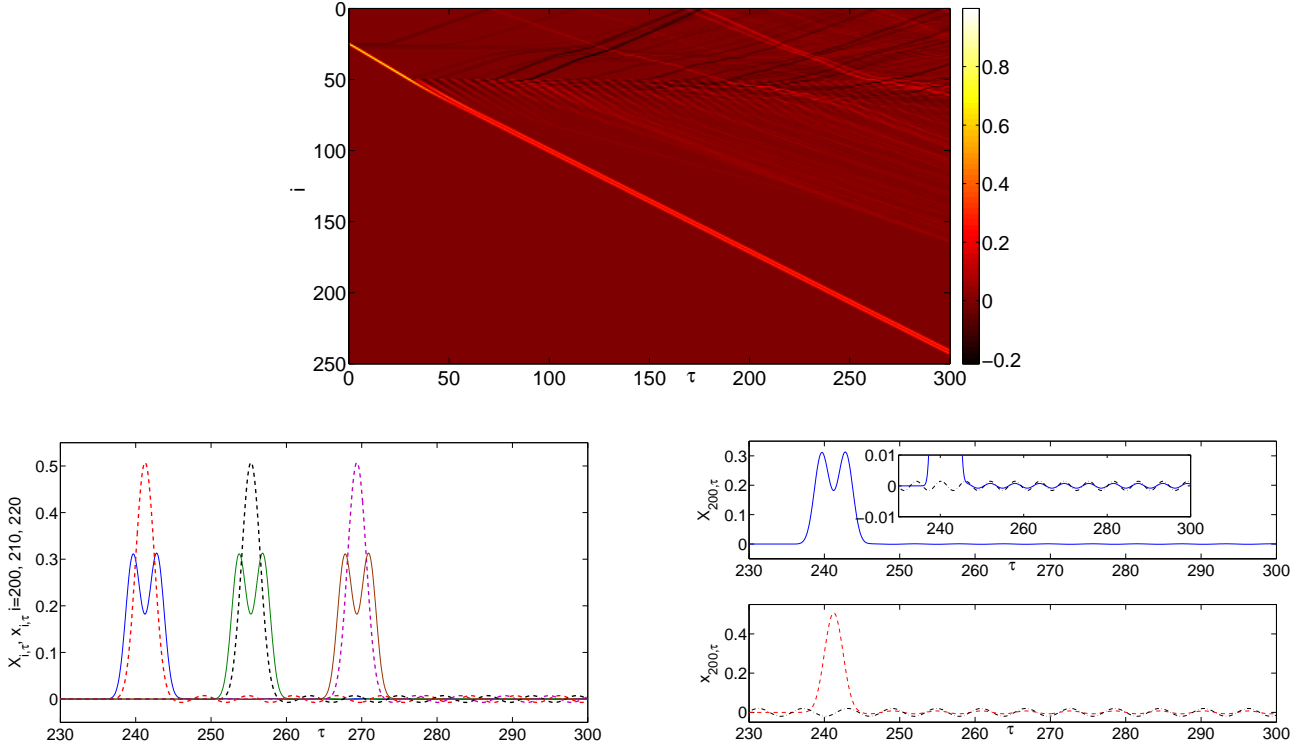


FIG. 12: The top panel shows the space-time contour plot of $\tilde{X}_{i,\tau}$, the time derivative of the displacement of the outer shell of our granular chain for $\tilde{\varepsilon} = 0.105$ and $\nu = 0.10245$. The particular evolution for 3 sites ($i = 200$ leftmost, $i = 210$ middle and $i = 220$ rightmost) are shown in the bottom left panel. The velocity of the the outer shells are given by the solid lines, while the dashed ones provide the evolution of the inner attachments. The presence of the oscillating tails is evident and is rendered more transparent in the right panel for site $i = 200$, where the outer shell field $\tilde{X}_{i,\tau}$ (top) is separated from the inner attachment field $\tilde{x}_{i,\tau}$ (bottom). Both of them oscillate and for comparison a dash-dotted sinusoidal curve with amplitude comparable to their tail oscillation amplitude and frequency selected as $\omega = \sqrt{\kappa(1 + 1/\nu)}$ is explicitly given to illustrate indeed the precise agreement of the tail oscillation with the frequency of the out-of-phase motion between the inner and outer beads. For the outer shell, the oscillation is not visible on the scale of the plot, and hence is given in the relevant inset which is a blowup at a proper scale to render it visible.

additional excitations stem from the reflection of this bead at a later stage). At the interface, a significant amount of excitations is produced which is visible (and is sustained thereafter) in the space-time contour plot of the velocity field $\tilde{X}_{i,\tau}$. This leads to the decay of the primary pulse, and the formation of a secondary one. However, shortly thereafter, the interference of the primary and secondary pulse distill a coherent waveform that appears to detach itself from residual “radiation” and to travel faster than the latter towards beads of higher index i . Observation of the contour plots, as well as of Figure 11 initially appears to suggest that the solitary wave is a genuinely localized one.

Nevertheless, this observation is *misleading*, as is revealed by the bottom panels of Figure 12 and the right panel of Figure 13. In particular, the same features as indicated above in Figure 11 are evident in the evolution of the time derivative of the displacement at the sites $i = 200$, $i = 210$ and $i = 220$. Yet, there are also clearly discernible tails which are highly ordered and follow the primary pulse. As the arbitrary oscillations, shown for comparison by the dash-dotted lines, suggest, the tail of the wave oscillates with *precisely* the natural linear frequency of the system, namely the frequency of the out-of-phase oscillator of the outer shell and its inner linear attachment, namely with $\omega = \sqrt{\kappa(1 + 1/\nu)}$. This is true for both examples (with very distinct linear frequencies due to the difference in the values of ν) of the bottom panels of Figure 12 and the right panel of Figure 13.

The above features constitute a significant new development. It is clear from the figures that an excitation propagates in the chain *without visible distortion* or attenuation, being preserved as a *weakly nonlocal solitary wave*. The latter waves, also known as nanoptera, constitute a type of waveform that in addition to a strongly localized core bears an extended tail. This is a theme of research that has attracted a considerable volume of activity from a wide range of areas including fluid mechanics, nonlinear optics and oceanography among others [35, 40], as well as from

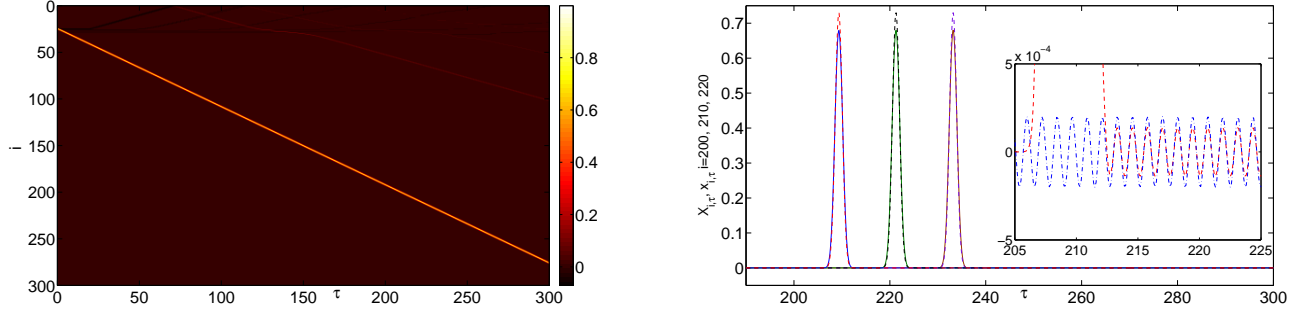


FIG. 13: Same as the previous figure, but now for the case of the single humped primary pulse for parameters $\tilde{\epsilon} = 0.105, \nu = 0.004$. In this case, as well, the right panel and specifically its inset and its comparison to an arbitrary sinusoidal curve with frequency $\omega = \sqrt{\kappa(1 + 1/\nu)}$ allow us to appreciate the existence of a tail oscillating with the above linear frequency.

the mathematical physics associated with exponential (and other types of) asymptotics [40, 41].

Hence, we devote the next section to an attempt to produce such coherent structures as exact traveling waves in our mass-in-mass chains.

V. NANOPTERONIC SOLUTIONS IN THE SYSTEM

Here, we will showcase a proof-of-principle example of the analysis and computation of nanopteronic waves of the type identified in the previous section, as well as of its uninhibited propagation through the granular crystal. In what follows, we will focus on nanoptera which have symmetric tails on both the “front” and the “back” of the main core, but the numerical computations of the previous section suggest that such entities can be quite long-lived even in the asymmetric case where they bear a “single arm”. More specifically, the nature of our initial conditions in section IV is not conducive to the formation of weakly localized nonlinear waves with such symmetric tails, but only to ones with a single arm/tail. However, as will be evident also from the numerical results herein, this is inconsequential as the core and the tail travel at the same speed, forming a coherent traveling structure.

Let us focus on the system of equations for the strains (where for simplicity we have set $\kappa = 1$, although this can straightforwardly be restored):

$$\Delta_{i,\tau\tau} = \left(\Delta_{i+1,+}^{3/2} + \Delta_{i-1,+}^{3/2} - 2\Delta_{i,+}^{3/2} \right) - (\Delta_i - d_i) \quad (33)$$

$$\nu\delta_{i,\tau\tau} = -(d_i - \Delta_i). \quad (34)$$

If we consider waves that spatially decay, in the regime of small amplitude, we can always identify wave amplitudes Δ_i (and δ_i) small enough such that $\Delta_i \gg \Delta_i^{3/2}$. Hence, it will always be the case that for small enough amplitudes, the relevant equations governing the evolution of the wave can be approximated as $\Delta_{i,\tau\tau} = -(\Delta_i - d_i)$ and $d_{i,\tau\tau} = -(1/\nu)(d_i - \Delta_i)$. These equations lead to $d_i = -\Delta_i/\nu$ and Δ_i satisfies the effective oscillator equation $\Delta_{i,\tau\tau} = -(1 + 1/\nu)\Delta_i$. Hence, it is natural to expect for small amplitude vibrations left behind a propagating wave with an oscillation of temporal frequency $\omega = \sqrt{1 + 1/\nu}$; in the presence of κ , this frequency becomes $\sqrt{\kappa(1 + 1/\nu)}$.

A. The Pego-English Approach and the Existence of Nanoptera

We now seek traveling waves of speed c to the dynamical equations in the form $\Delta_i(t) = R(i-ct)$ and $d_i(t) = S(i-ct)$, substituting these expressions in (33) and (34). The resulting advance-delay differential equations in the traveling wave variable $\xi = i - ct$ are then of the form:

$$c^2 R''(\xi) = \left[R(\xi + 1)_+^{3/2} + R(\xi - 1)_+^{3/2} - 2R(\xi)_+^{3/2} \right] - (R(\xi) - S(\xi)) \quad (35)$$

$$c^2 \nu S''(\xi) = -(S(\xi) - R(\xi)), \quad (36)$$

where the prime denotes derivative with respect to its argument. We now use the Fourier transform of these equations according to the definition $\hat{R}(k) = (1/2\pi) \int_{-\infty}^{\infty} R(\xi) e^{ik\xi} d\xi$ (and similarly for S). We thus obtain in this generalization

of the approach used in [27] the following conditions (upon writing the relevant algebraic equations and solving them for \hat{R} and \hat{S})

$$\hat{R} = \frac{1 - \nu c^2 k^2}{1 + \nu - \nu c^2 k^2} \left(\frac{\sin(\frac{k}{2})}{c \frac{k}{2}} \right)^2 \widehat{(R^{3/2})} \quad (37)$$

$$\hat{S} = \frac{1}{1 - \nu c^2 k^2} \hat{R}. \quad (38)$$

As a side note, we should mention here that in the infinite lattice the above equations should be considered in the sense of distributions, given the non-vanishing nature of the tails. Nevertheless, in what follows, we will restrict our considerations to a finite domain.

The above equations can be considered as an iterative scheme that can be used computationally in order to retrieve its fixed point (nontrivial) solution that would constitute the traveling wave of the original dynamical (strain) equations. In particular, given a profile R , the right hand side of (37) is computed and used to obtain the next order guess for \hat{R} , whose subsequent use in (38) and Fourier transform of both \hat{R} and \hat{S} will give rise to the next order guesses, and so on, till convergence. Naturally, for $\nu = 0$, this iteration scheme retrieves the one used to obtain the solitary waves of the monoatomic granular chain in [27].

An additional possibility which would avoid the complications (slow tail decay in Fourier space) of the Fourier calculation proposed above would be to revert (37) and (38) into real space. That would reduce the number of modes needed for an accurate computation of the solution. In the present computation, a large number of modes is used over domains of size 120 or even 240, with $dx = 0.01$ and periodic boundary conditions (although only a small fraction of the lattice is shown for clarity).

A typical example of the result of the iteration scheme of (37) and (38) is given in Figures 14 and 15 for the case of $\nu = 0.05$. Figure 14 illustrates the result of the iterative scheme of the equations towards the acquisition of a traveling wave solution.

It is not only interesting that the scheme continues to converge for this finite value of ν . It is, in fact, remarkable that, as is partially anticipated from the argument of the previous sections (and from our results illustrating the attenuation of a regular monotonic pulse and the spontaneous emergence of such weakly nonlocal solitary waves), the obtained exact solutions have a *nanopteronic* character. Namely, they feature spatial oscillations with a period which is consonant with the dominant wavenumber (which is $(1/c)\sqrt{1+1/\nu}$ as illustrated in (37)). In the latter equation, the poles along the real k -axis arise precisely at $k_0 = (1/c)\sqrt{1+1/\nu}$, suggesting that the corresponding Cauchy principal value integral (arising when Fourier transforming to obtain $R(\xi)$), will naturally give rise to a sinusoidal dependence on $k_0\xi$. From (38), this is expected to be reflected in the spatial dependence of $S(\xi)$ as well. This, in turn, is consonant with the temporal oscillation featuring the frequency of the out-of-phase mode, as the corresponding frequency $\omega_0 = ck_0$ and hence is in agreement with the above numerical observations of Figures 12 and 13. This implies that there exists a resonance between the propagation of the traveling wave and the excitation of the linear out-of-phase mode of each resonator, a feature that has been analyzed in detail in [42]. In fact, in the latter work, additionally a so-called antiresonance condition (of $k = 2n\pi$) was also identified under which a regular solution with monotonically decaying tail was identified. Only in this case of anti-resonance has it recently been proved that a solution in this resonator chain exists (and is bell-shaped) [43]. Admittedly, the proof of convergence of the above scheme in the case of nanoptera with non-vanishing tails is an important open problem (as is the rigorous mathematical proof of existence of such states).

While $R(\xi)$ and $S(\xi)$ are obtained as continuum solutions in the left panel of the figure, they are “distilled” on the lattice in the right panel and so is the corresponding lattice momentum associated with the chosen speed of $c = 1$.

Subsequently, such nanoptera are “released” on the lattice and are found to indeed propagate with the prescribed speed of $c = 1$, *without modifying their nanopteronic character*, as is clearly demonstrated for over 100 time (and space) units in Figure 15. The figure shows the two strain fields $\Delta_i(t)$ and $d_i(t)$ as contour plots of space i and time t and the unit slope propagation is clearly indicative of their robustness. The initial and final profiles of the two fields are shown in the left insets (of the left and right panel, respectively). The right insets indicate the evolution of the maximum of the field as a function of time. Both insets reveal the unscathed traveling nature of the resulting waveforms. The tails are evident in the logarithmic scale evolution of the strain fields shown in the bottom panels.

VI. CONCLUSIONS AND FUTURE CHALLENGES

In the present work, we have studied the wave propagation in a novel granular structure which consists of a chain of hollow beads interacting via Hertzian contacts, and containing linear resonators. We have seen that such a local

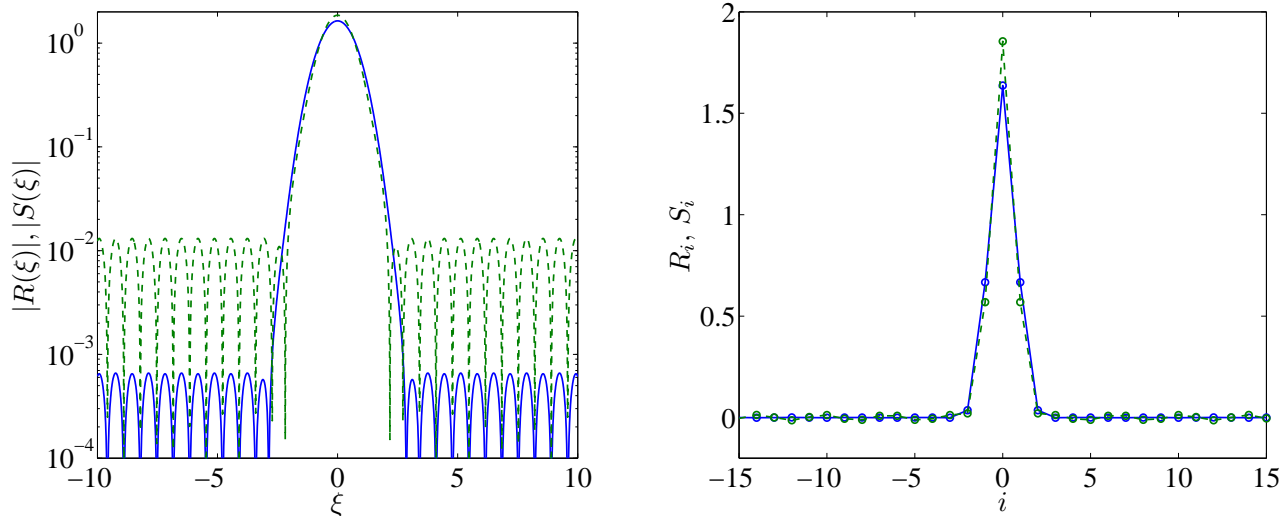


FIG. 14: The left panel shows the solution of the continuum iterative processing of (37) and (38) in the co-traveling frame with $c = 1$ for the fields R and S as functions of ξ . The right panel identifies the values of the field ordinates on the sites i of the lattice. R_i is shown by the circles connected by the solid (blue) line, while S_i by the circles connected by the dashed (green) line.

oscillator provides a gateway for the energy of the primary traveling pulses, well-known to propagate unimpeded in the regular elastic chain, to be gradually removed. This leads to a systematic decrease of the pulse’s amplitude. Adapting the recent method of [31] to this complex, non-autonomous case, we were able by means of ODE techniques (solving for the attachment and back-substituting in the shell equation, assuming a decaying pulse in the shell equation and integrating it between suitable instants in time) to capture the pulse’s decrease of amplitude. This was done by a nonlinear map approach that was found to be highly efficient, under suitable assumptions. It is important to note, that the similar approach with modification has been applied in [39], and its results were found very efficient in depicting the evolution of the primary pulse amplitude.

Nevertheless, this amplitude and pulse decay were not the sole features of this novel chain. Instead, such decay gave rise to the emergence of secondary pulses that eventually overtake the primary pulse, leading to a modulated waveform. Under suitable conditions, this modulated waveform was found to self-organize into a robust traveling wave that detached from the background “radiation” and was observed to propagate unhindered (and with constant amplitude and speed) through the lattice. These waves were studied in more detail and were identified as weakly nonlocal solitary waves i.e., nanoptera. A formulation of the existence problem of such waves was provided in Fourier (and real) space which enabled the identification of their dominant wavenumber k_0 and of their temporal frequency of tail oscillation $\omega = ck_0$, as well as its exact proof-of-principle computation. The frequency of tail oscillation was identified as the frequency of the relative out-of-phase oscillation of the outer shell and the inner attachment.

Naturally, this study opens a number of new directions that are worthy of examination in their own right. For instance, it would be particularly interesting to explore in their own right the nanopteronic solutions of the model from a rigorous mathematical perspective and establish their regularity and stability properties, as well as to develop robust numerical schemes for identifying such coherent structures bearing a spatial tail.

Going beyond the present model, one of the critical assumptions herein was that the oscillator connecting the outer shell and inner attachment is linear. It would be interesting to explore the possibility of soft or hard anharmonic oscillators and to examine the fate of the nanoptera in the presence of such anharmonicity. It is tempting to conjecture that they would persist on the basis of the argument associated with the solitary wave tails, yet a systematic study of the properties of such waves would certainly be warranted.

On the other hand, here we have restricted our considerations to the “highly nonlinear” limit (from the point of view of the outer shell Hertzian interactions). In that light, we have assumed that the shells do not sustain an external, so-called pre-compression, force. Yet, the existence of such pre-compression would provide a linear limit to the problem that is of particular interest in its own right in such mass-in-mass “metamaterials”. The examination of the linear and nonlinear properties of pre-compressed crystals would be a topic for future studies in its own right. A particularly relevant feature to explore in this context stems from the comparison with [29]. There it was found that the models with precompression spontaneously produce nanoptera with oscillations on both sides, while in the absence of precompression, only ones with extended waves on one side arose. It would be interesting to explore a

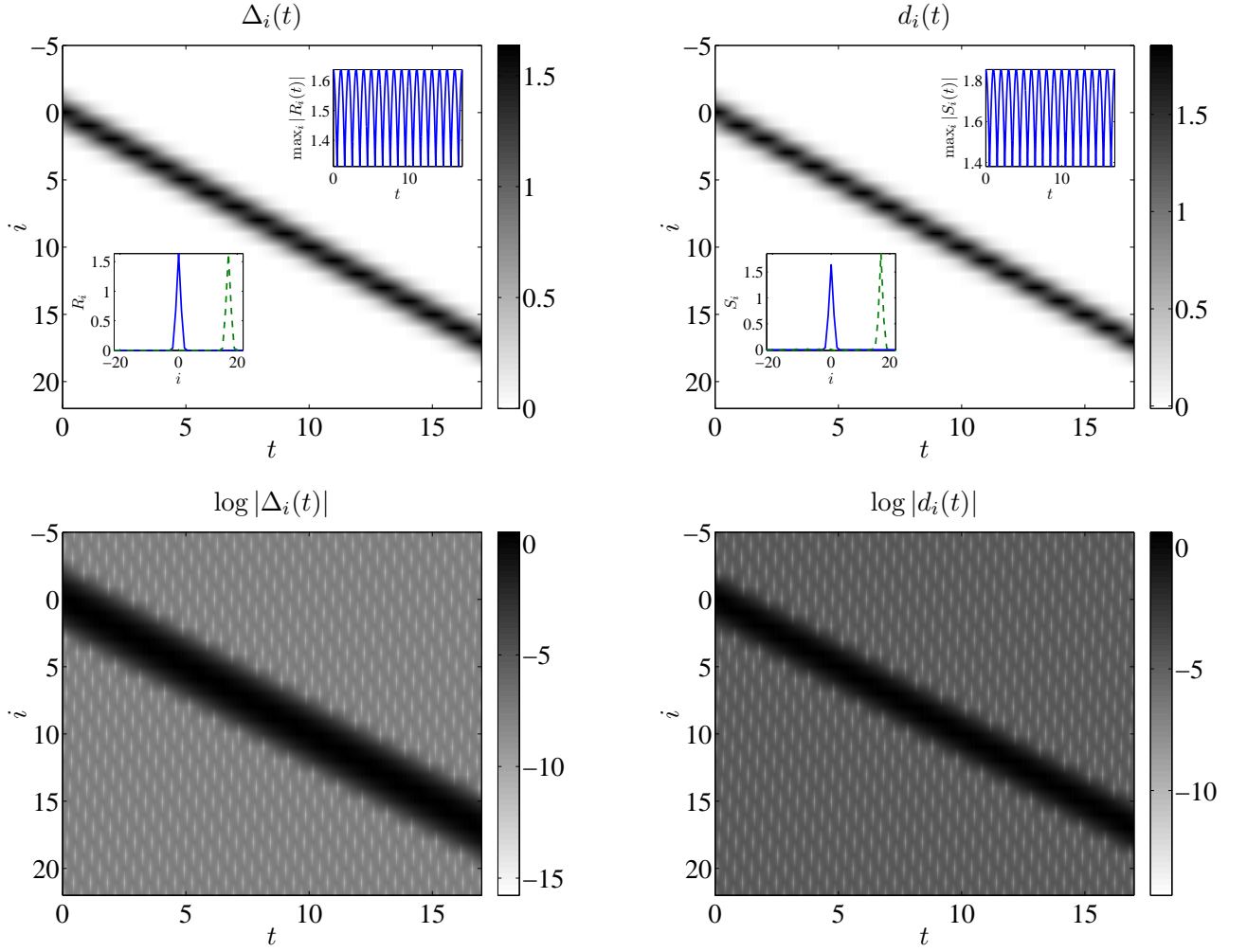


FIG. 15: The evolution of the two fields $\Delta_i(t)$ and $d_i(t)$ for nanopertion initial conditions in the case of $\nu = 0.05$ and unit speed (notice the propagation slope). The right insets show the time oscillation of the solution maximum, while the left ones show the initial and final solution configurations revealing their robust propagation. The bottom panels illustrate the logarithmic scale of the relevant evolution, rendering clear the presence of the tails.

systematic comparisons with these findings.

These themes are currently under investigation and will be reported in future works.

Acknowledgements. P.G.K is grateful to Ricardo Carretero and Haitao Xu for some technical assistance with some of the figures. He also gratefully acknowledges support from US-ARO under grant W911NF-15-1-0604 and from US-AFOSR under grant FA-9550-12-1-0332. G.T. acknowledges financial support from FP7-CIG (Project 618322 ComGranSol).

-
- [1] V. F. Nesterenko, *Dynamics of Heterogeneous Materials*, Springer, New York, (2001).
 - [2] V. F. Nesterenko, Propagation of nonlinear compression pulses in granular media, *J. Appl. Mech. Tech. Phys.*, **24**, 5, (1984).
 - [3] K. Ahnert and A. Pikovsky Compactons and chaos in strongly nonlinear lattices, *Phys. Rev. E* **79**, 026209 (2009).
 - [4] A. Chatterjee, Asymptotic solution for solitary waves in a chain of elastic spheres, *Phys. Rev. E* **59**, 5912 (1999).
 - [5] A. N. Lazaridi and V. F. Nesterenko, Observation of a new type of solitary waves in a one-dimensional granular medium, *J. Appl. Mech. Tech. Phys.* **26**, 405, (1985).
 - [6] C. Coste E. Falcon, S. Fauve, Solitary waves in a chain of beads under Hertz contact, *Phys. Rev. E* **56**, 6104 (1997).
 - [7] R. S. MacKay, Solitary waves in a chain of beads under Hertz contact, *Phys. Lett. A* **251**, 191, (1999).

- [8] J.Y. Ji and J. Hong, Existence criterion of solitary waves in a chain of grains, *Phys. Lett. A* **260**, 60 (1999).
- [9] R. Doney and S. Sen, Decorated, Tapered, and Highly Nonlinear Granular Chain, *Phys. Rev. Lett.* **97**, 155502 (2006).
- [10] U. Harbola, A. Rosas, M. Esposito, K. Lindenberg, Pulse propagation in tapered granular chains; an analytic study, *Phys. Rev. E* **80**, 031303 (2009).
- [11] K. Lindenberg, U. Harbola, A. H. Romero, A. Rosas, Pulse propagation in granular chains, *AIP Conf. Proc.* **1339**, 97 (2011).
- [12] G. Theocharis, N. Boechler, P.G. Kevrekidis, S. Job, M. A. Porter, and C. Daraio, Intrinsic energy localization through discrete gap breathers in one-dimensional diatomic granular crystals, *Physical Review E*, **82**, 056604 (2010).
- [13] G. Theocharis, M. Kavousanakis, P. G. Kevrekidis M. A. Porter, C. Daraio, I.G. Kevrekidis, Localized breathing modes in granular crystals with defects, *Physical Review E* **80**, 066601 (2009).
- [14] N. Boechler, G. Theocharis, S. Job, M.A. Porter, P.G. Kevrekidis, C. Daraio, Discrete breathers in one-dimensional diatomic granular crystals *Physical Review Letters* **104**, 244302, (2010).
- [15] Y. Starosvetsky, K. R. Jayaprakash, A.F. Vakakis, Scattering of Solitary Waves and Excitation of Transient Breathers in Granular Media by Light Intruders and no Precompression, *J. Appl. Mech.* **79**, 011001 (2012).
- [16] K.R. Jayaprakash, Y. Starosvetsky A.F. Vakakis New Family of Solitary Waves in Granular Dimer Chains with no Precompression, *Phys. Rev. E.* **83**, 036606 (2011).
- [17] M. A. Porter, C. Daraio, I. Szelengowicz, E. B. Herbold, P. G. Kevrekidis, Highly Nonlinear Solitary Waves in Periodic Dimer Granular Chains, *Phys. Rev. E.* **77**, 015601, (2008).
- [18] E.B. Herbold, J. Kim, V.F. Nesterenko, S.Y. Wang, and C. Daraio, Pulse propagation in a linear and nonlinear diatomic periodic chain: effects of acoustic frequency band-gap, *Acta Mechanica* **205**, 85 (2009).
- [19] E. B. Herbold, V. F. Nesterenko, and C. Daraio, Influence of Controlled Viscous Dissipation on the propagation of Strongly Nonlinear Waves in Stainless Steel Based Phononic Crystals, in Shock compression of condensed matter 2005, Proceedings of the Conference of the American Physical Society Topical Group on Shock Compression of Condensed Matter, AIP Conference Proceedings **845**, edited by M.D. Furnish, M. Elert, T.P. Russel, and C.T. White, American Institute of Physics, Melville, New York, pp. 1523 (2006).
- [20] E.B. Herbold, V.F. Nesterenko, Shock wave structure in a strongly nonlinear lattice with viscous dissipation, *Phys. Rev. E* **75**, 021304 (2007).
- [21] E.B. Herbold, V.F. Nesterenko, The role of dissipation on wave shape and attenuation in granular chains, *Physics Procedia* **3** (1), 465 (2010).
- [22] M. Manciu, S. Sen and A. Hurd, Impulse propagation in dissipative and disordered Hertzian |chains, *Physica D* **157**, 226 (2001).
- [23] R. Carretero-González, D. Khatri, M. A. Porter, P. G. Kevrekidis, C. Daraio, Dissipative Solitary Waves in Granular Crystals, *Phys. Rev. Lett.* **102**, 024102 (2009).
- [24] A. Rosas, A.H. Romero, V. F. Nesterenko, K. Lindenberg, Short pulse dynamics in strongly nonlinear dissipative granular chains, *Phys. Rev. E* **78**, 051303 (2008).
- [25] G. Friesecke and J. A. D. Wattis, Existence theorem for solitary waves on lattices, *Commun. Math. Phys.* **161**, 391 (1994).
- [26] A. Stefanov and P.G. Kevrekidis, On the Existence of Solitary Traveling Waves for Generalized Hertzian Chains, *J. Nonlin. Sci.* **22**, 327 (2012).
- [27] J.M. English and R.L. Pego, On the solitary wave pulse in a chain of beads, *Proceedings of the AMS* **133**, 1763 (2005).
- [28] G. James, Nonlinear waves in Newton's cradle and the discrete p- Schrödinger equation, *Math. Mod. Meth. Appl. Asc.* **21**, 2335 (2011).
- [29] G. James, P. G. Kevrekidis, J. Cuevas, Breathers in oscillator chains with Hertzian interactions, *Phys. D* **251**, 39 (2013).
- [30] S. Job, F. Santibanez, F. Tapia, and F. Melo, Wave localization in strongly nonlinear Hertzian chains with mass defect, *Phys. Rev. E* **80**, 025602 (2009).
- [31] Y. Starosvetsky, Evolution of the primary pulse in one-dimensional granular crystals subject to on-site perturbations: Analytical study, *Phys. Rev. E* **85**, 051306 (2012).
- [32] L. Bonanomi, G. Theocharis, C. Daraio, Wave propagation in granular chains with local resonances, *Phys. Rev. E* **91**, 033208 (2015).
- [33] L. Liu, G. James, P.G. Kevrekidis, and A. Vainchtein, *Nonlinear waves in a strongly nonlinear resonant granular chain*, *Nonlinearity* **29**, 3496 (2015).
- [34] L. Liu, G. James, P.G. Kevrekidis, and A. Vainchtein, *Breathers in a locally resonant granular chain with precompression*, *Physica D: Nonlinear Phenomena* **331**, 27 (2016).
- [35] J.P. Boyd, *Weakly Nonlocal Solitary Waves and Beyond-All-Orders Asymptotics*, Kluwer Academic Publishers, Dordrecht (1998).
- [36] G. Iooss, *Chaos* **15**, 015113 (2005).
- [37] D. Ngo, S. Griffiths, D. Khatri, and C. Daraio, Highly nonlinear solitary waves in chains of hollow spherical particles, *Gran. Mat.*, in press (2013).
- [38] P. G. Kevrekidis, A. Vainchtein, M. Serra Garcia, and C. Daraio *Phys. Rev. E* **87**, 042911 (2013).
- [39] Y. Ben-Meir, and Y. Starosvetsky, Modulation of solitary waves and formation of stable attractors in granular scalar models subjected to on-site perturbation, *Wave Motion* **51** 685-715 (2014).
- [40] J.P. Boyd, *The Devil's Invention: Asymptotics, Superasymptotic and Hyperasymptotic Series*, *Acta Applicandae* **56**, 1 (1999).
- [41] E. Lombardi, *Oscillatory integrals and phenomena beyond all algebraic orders; with applications to homoclinic orbits in reversible systems*. Lecture Notes in Mathematics, Springer-Verlag, vol. 1741, (Berlin, 2000).

- [42] H. Xu, P.G. Kevrekidis, and A. Stefanov, *Traveling waves and their tails in locally resonant granular systems*, J. Phys. A: Math. Theor. **48**, 195204 (2015).
- [43] P.G. Kevrekidis, A.G. Stefanov and H. Xu, *Traveling Waves for the Mass in Mass Model of Granular Chains*, Lett. Math. Phys. **106**, 1067 (2016).
- [44] Y. Starosvetsky, and A.F. Vakakis, *Traveling Waves and Localized Modes in One-dimensional Homogeneous Granular Chains with no Pre-compression*, Phys. Rev. E **82** 026603 (2010).

VII. APPENDIX

It should be noted in passing here that a very accurate, analytically tractable Padé approximation of the primary pulse wave has been derived recently in [44] in the form

$$\tilde{S}(\tau) \cong \left(\frac{1}{q_0 + q_2\tau^2 + q_4\tau^4 + q_6\tau^6 + q_8\tau^8} \right)^2, \quad (39)$$

where $\tilde{S}(\tau)$ denotes the normalized (with respect to a time shift) solitary wave solution of the homogeneous granular chain, τ is a normalized time, q_0, q_2, q_4, q_6, q_8 are universal constants given explicitly in [44].

Unfortunately, this functional form of the solitary pulse is rather cumbersome and leads to the unnecessary complications in the analysis devised in the present study. Thus, to overcome this difficulty in the present study the approximation of the solitary wave profile is sought in the following functional form

$$\Delta_i^s(\tau) = S^s(\tau - i) = \begin{cases} B \cos^4(\alpha(\tau - i)), & \tau \in [i - \frac{\pi}{2\alpha}, i + \frac{\pi}{2\alpha}] \\ 0, & \text{otherwise} \end{cases} \quad (40)$$

The theoretical procedure of finding the fitting parameters B and α comprises the following two rather simple stages. At the first stage we assign the amplitude to be equal to the amplitude of the particular, exact, solitary wave solution propagating with the unity phase shift ($B = 1.4954$). This value can be easily deduced from either numerical simulations or semi-analytical techniques e.g. the English-Pego procedure [27]. The second fitting parameter is computed by equating the areas covered by the exact and the approximated solitary wave profiles, yielding the following simple algebraic relation.

$$\alpha = \frac{3\pi B}{8 \int_{-\infty}^{+\infty} S_{\text{exact}}(\tau) d\tau} = 0.6446. \quad (41)$$

In fact, the derived parameters α and B can be considered as universal, as due to the homogeneity of the nonlinear lattice under investigation, the derived approximation can be properly scaled to fit to the arbitrary solitary wave profile, having the following form.

$$S_i(\tau) = AS^s(A^{1/4}\tau - i) \quad (42)$$

Here A is the ratio between the amplitude of the arbitrary, solitary wave profile and the normalized one ($S^s(0)$). The comparison between the exact solution and the approximate solution is illustrated in Figure 16.

We can see that this approximation is fairly adequate throughout the support of the relevant wave.

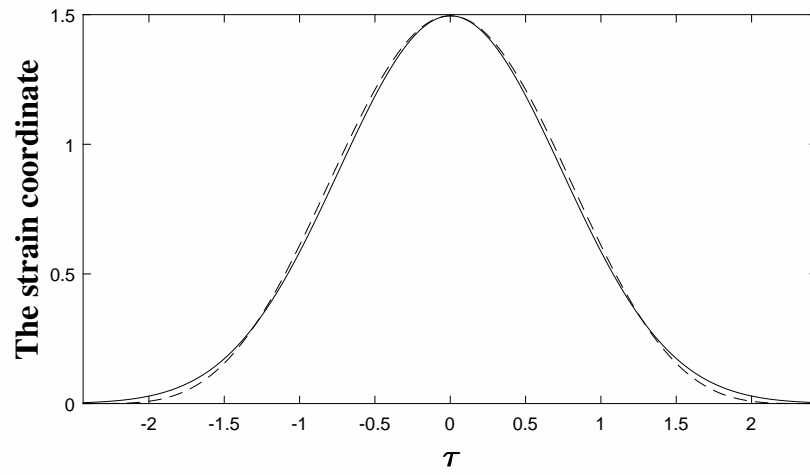


FIG. 16: The comparison between the exact solution and the approximate one (40). The solid line shows the exact solution and the approximate one is denoted by the dashed line.